Simulation of Single Mode Si Waveguides and Electro-Optic Coupling Modulators

by

Desmond Rodney Lim

Submitted to the Department of Electrical Engineering in partial fulfillment of the requirements for the degree of

Bachelor of Science in Electrical Science & Engineering

at the

MASSACHUSETTS INSTITUTE OF TECHNOLOGY

May 1994
[June 1994]

MASSACHUSETTS INSTITUTE OF TECHNOLOGY
JUN 15 1994
LIBRARIES
ARCHIVES

Copyright Desmond Rodney Lim, 1994. All rights reserved.

The author hereby grants to MIT permission to reproduce and to distribute copies of this thesis document in whole or in part, and to grant others the right to do so.

Author ....
Department of Electrical Engineering and Computer Science
May 6 1994

Certified by ....
Professor Lionel C Kimerling
Professor, Material Science Department
Thesis Supervisor

Accepted by ....
Leonard A. Gould
Chairman, Department Committee on Undergraduate Theses

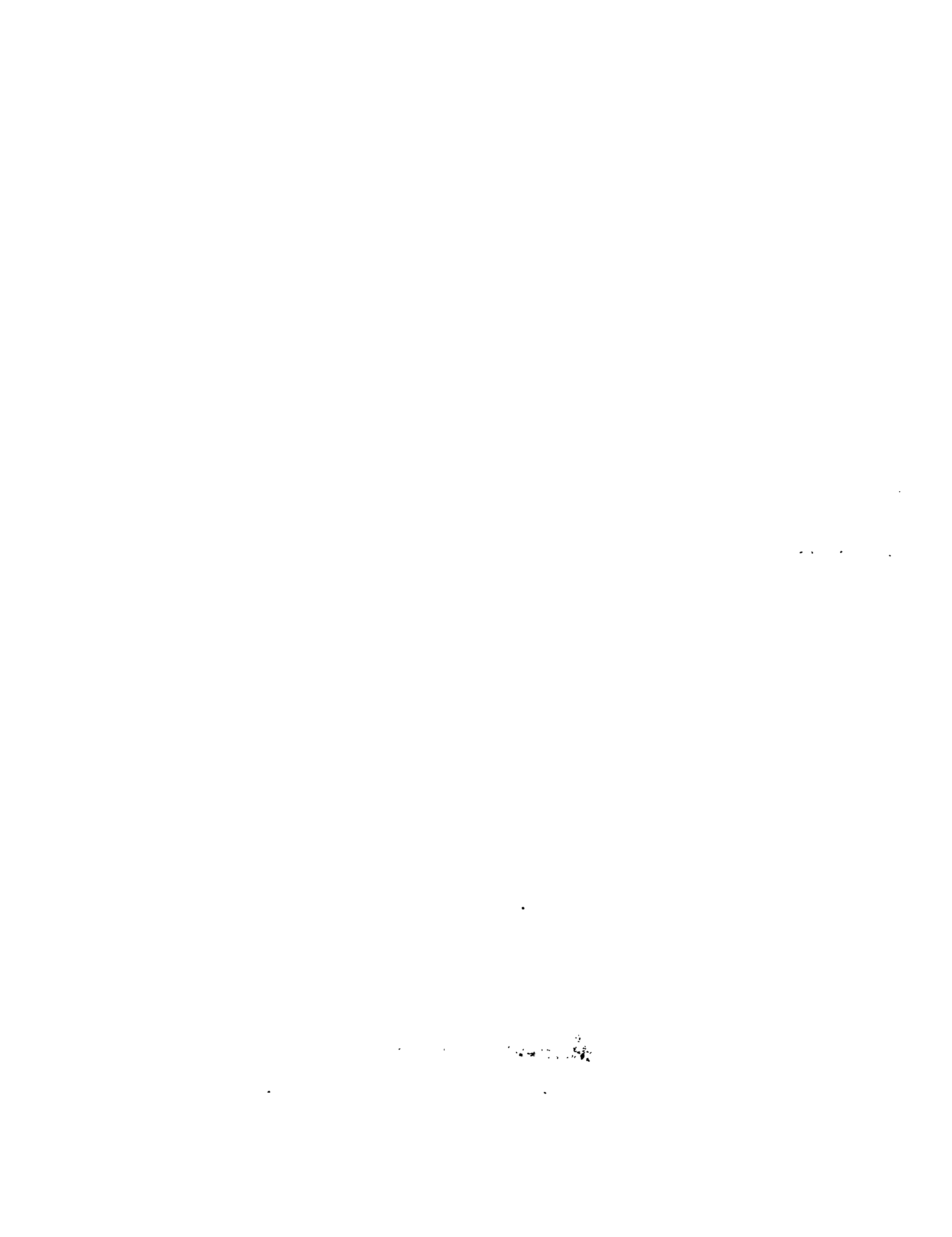

Simulation of Single Mode Si Waveguides and Electro-Optic Coupling Modulators

by

Desmond Rodney Lim

Submitted to the
Department of Electrical Engineering and Computer Science

May 6, 1994

In Partial Fulfillment of the Requirements for the Degree of Bachelor of Science in Electrical Science and Engineering

Abstract

Single mode strip and rib waveguides were simulated and evaluated in this report. In order to make these waveguides compatible with IC patterning techniques, dimensions on the order of 1 μm were considered for the waveguide design. An electro-optic modulator which operates by dielectric waveguide mode coupling was also investigated. The modulator design was based on a directional coupler of the rib waveguide structure and utilized the free carrier refraction effect to modulate the optical signal. A light source at 1.55 μm, which is close to the wavelength of peak emission of erbium in silicon, was used in the simulations.

Thesis Supervisor: Lionel C Kimerling
Title: Professor, Materials Science Department

Acknowledgments

I would like to express my deepest gratitude to my thesis advisor, Professor Kimerling, for his insight, patience and guidance, without which this thesis would have been impossible. I am also indebted to Debra Koker for providing me with valuable input on waveguide design and for her suggestions on improving this manuscript.

In addition, I would like to thank Professor Haus and Jerry Chen, for letting me use the beam propagation simulator at MIT, which was the primary analytical tool used in this thesis. Special thanks to Dr. Conor Rafferty, author of PROPHET, and Dr. Mark Pinto, author of PADRE for their kind permission to use these simulators. The beam propagation simulations were run on DEC Model 5000 and IBM PowerStation 320H computers in MIT's Athena computing environment, while PROPHET and PADRE simulations were run on a SUN SparcStation II and a CRAY YMP supercomputer at AT & T.

To the members of the Electronics Materials group, Bo, Frank, Hichem, Kate, Jim and Jurgen, who in one way or the other have helped me in this thesis, thank you.

Special thanks to Carla, Pam and Joanne, my mentors in Athena consulting, who provided invaluable computing support during the write-up.

Over the years, I have received support from my friends and I am unable to list all the friends who have helped keep me sane whilst I was writing this manuscript.

Words are insufficient to express my gratitude to my parents and my sister Leona, who have always been there to motivate me and to give me constant encouragement. Without their love and support, I would not have made it this far. Thank you.

Table of Contents

1 Introduction 11

2 Background and Theory 13

2.1 Background 13

2.2 Free Carrier Effect 14

2.3 Injection Mechanism 18

2.4 Dielectric Coupling Modulators 19

2.5 Simulations and Calculations 23

2.5.1 Waveguide and Eigenmode Simulations 23

2.5.2 Waveguide Bending Loss Calculations and Simulations 23

2.5.3 Process and Electrical Simulations 27

3 Waveguide Design 29

3.1 Waveguide Structures 29

3.2 Design Considerations 31

3.2.1 Strongly Confined vs. Weakly Confined Waveguides 31

3.2.2 Waveguide Losses 32

3.3 Rib Waveguide 34

3.3.1 Dimensions 34

3.3.2 Eigenmode Simulations 35

3.3.3 Loss to Substrate Simulations 36

3.3.4 Bending Loss Simulations 37

3.3.5 Loss to Metal Contact Simulations 42

3.3.6 Ease of Fabrication 44

3.4 Strip Waveguide 45

3.4.1 Dimensions 45

3.4.2 Eigenmode Simulations 45

3.4.3 Loss to Substrate Simulations 46
3.4.4 Bending Loss Simulations 48
3.4.5 Loss to Metal Contacts Simulations 49
3.4.6 Ease of Fabrication 52

4 Modulator Design 55

4.1 Rib Waveguide Coupling Modulator 55
4.1.1 Dimensions of Simulated Structure 55
4.1.2 Eigenmode Simulations of Rib Coupler 55
4.1.3 Simulation of Coupling in Rib Waveguides 57
4.1.4 Loss Simulations of the Rib Waveguide Coupler 64
4.1.5 Process Flow and Process Simulations 66
4.1.6 Electrical Simulations 71

4.2 Strip waveguide modulator 77

5 Conclusion and Recommendations 81

5.1 Rib and Strip Waveguides 81
5.2 Modulators 82
5.3 Future Work 82
5.3.1 Metal Contact vs. Bending Losses 83

Bibliography 87

List of Figures

Figure 2.1: Graph showing the free carrier refraction effect at λ=1.55 μm (from reference.[6]) ... 15

Figure 2.2: Graph showing free carrier absorption effect at λ=1.55 μm (from reference [6]) ... 17

Figure 2.3: Cross sectional view of the generalized index profile and field pattern ... 19

Figure 2.4: Schematic showing waveguide coupling ... 21

Figure 2.5: Schematic of radiation loss due to waveguide bending ... 24

Figure 2.6: Schematic of conformal map as proposed by Heiblum et.al. [23] ... 25

Figure 3.1: Schematic of a strip waveguide ... 29

Figure 3.2: Schematic of the rib waveguide ... 30

Figure 3.3: Schematic of the Si-Ge waveguide ... 30

Figure 3.4: Cross section of a rib waveguide of dimensions 3 μm by 5 μm, r=0.5 and eigenmode of the guided mode. (Simulation of 140x90 points, scale 10pts:1 μm) ... 35

Figure 3.5: Simulation of loss to substrate in rib waveguides for heights between 2 μm & 5 μm and widths between 1 μm & 3 μm (r=0.5; oxide thickness =0.2 μm). ... 37

Figure 3.6: Bending loss in dB/cm for rib waveguides of various dimensions vs. bending radius in μm using Marcuse's approximation. See text. ... 38

Figure 3.7: Schematic showing how the transformed index profile changes with radius of curvature. ... 40

Figure 3.8: Schematic of the three waveguide coupler ... 41

Figure 3.9: Schematic of the cross coupler ... 42

Figure 3.10: Simulation of loss to substrate in rib waveguides for heights between 2 & 5 μm and widths between 1 & 3 μm with top metal contacts (oxide thickness=0.2 μm). ... 43

Figure 3.11: Eigenmode of the strip waveguide with dimensions of 0.2 μm x 0.5 μm (Simulation of 80x100 points, scale 40 pts:1 μm) ... 46

Figure 3.12: Loss in dB/cm vs. oxide thickness in μm for strip waveguides ... 47

Figure 3.13: Bending loss in dB/cm for strip waveguides of various dimensions vs.

bending radius in μm 48

Figure 3.14: Schematic of "Finger" contacting scheme 50

Figure 3.15: Schematic of contacting 51

Figure 4.1: First eigenmode of rib waveguide coupler with width = 3 μm and height = 5 μm (Simulation of 140x80 points, scale 10pts:1 μm) 56

Figure 4.2: Plot showing coupling of E field in rib waveguide ($\Delta n=0$) 58

Figure 4.3: Plot showing coupling of E field in rib waveguide ($\Delta n=-3x10^{-3}$) 59

Figure 4.4: Graph showing the evolution of E field with $\Delta n=0$ 60

Figure 4.5: Graph showing the evolution of E field with $\Delta n=-3x10^{-3}$. 62

Figure 4.6: Plot of loss in dB to substrate, carrier injection and metal vs. propagation distance 65

Figure 4.7: Schematic of process flow for rib waveguide modulator (not drawn to scale) 67

Figure 4.8: Result of the 2 D Prophet simulation 69

Figure 4.9: Padre simulation of hole concentration at an applied voltage of V=0V 72

Figure 4.10: Padre simulation of hole injection concentration when the p-i-n device is in the on state or voltage drop between the p+ and n+ contacts is 1.2V 73

Figure 4.11: Simulation of hole concentration of the device in waveguide II. The applied voltage V=1.2V is turned at on $t=0^{+}$ns and then turned off at t=30ns. The system returns to V=0V state by t=50ns. 74

Figure 4.12: Simulation of hole concentration of the device in waveguide I. The applied voltage V=1.2 V is turned on at $t=0^{+}$ns and then turned off at t=30ns. The system returns to V=0V state by t=50ns. 75

Figure 4.13: Plot of coupling length in μm vs. waveguide separation in μm for a strip waveguide coupler with strip dimensions 0.2 μm vs. 0.5 μm 78

Figure 5.1: Schematic of SiGe in Si waveguides which should show low bending loss and loss to metal contacts 84

Chapter 1

Introduction

Integrated electro-optics is of interest as it combines the computing power of electronics with the communications applications of optical networks. Although silicon is the most important substrate in microelectronics industry, it does not have many useful optical properties. For example, since it is centro-symmetric, the Pockels effect is negligible in silicon [1] and since it is not a direct band gap material, the light emission efficiency of silicon is poor. Nevertheless, there is still much interest in developing silicon electro-optics because it provides a means to alleviate the problems of clock skew and interconnect limitations in VLSI/ULSI technology. This project is part of a larger undertaking by the Electronic Materials group to study the possibility of integrated optical and electronic devices on silicon.

The goal of this thesis is to study waveguides and electro-optic modulators in silicon. Waveguides and modulators are important components in optoelectronics. Several waveguide structures, including single mode strip and rib waveguides are considered and are evaluated in this report.

A possible modulator design based on the rib waveguide structure is proposed. The modulator will be based on the directional coupler design and will use the free carrier effect for modulation of the optical signal. The design will be compatible with a light source at 1.55 μm, which is close to the wavelength of peak emission of erbium in silicon. The purpose of this study is to determine a modulator design which is readily integrable with silicon-erbium optoelectronic technology [2-5]. In addition, since the modulator is a

relatively simple device, designing and fabricating such a device may help elucidate some problems with more complicated devices.

This document first describes the physical effects which will be used in the design of the waveguides and the modulators. This is followed by a discussion of the simulators which were used to study the waveguides and the modulators. The results of the simulations of the waveguides are presented next. Finally, an analysis of the results of simulations of the modulator will be detailed.

Chapter 2

Background and Theory

2.1 Background

In order to develop optoelectronics in silicon, three important components

- the light source (laser diodes and light emitting diodes),
- the transmission devices (waveguides and modulators) and
- the optical detectors

must first be developed. The design of a silicon waveguide and electro-optic modulator system will depend on the successful design of an efficient light source in silicon. Rare earth doping, specifically Er doping, has been proposed as a promising technology for efficient light emission in silicon [3-5]. Recently Zheng et al. reported the first room temperature sharp line electroluminescence of an erbium doped silicon light emitting diode (LED) [2]. Thus, the modulator that I will be presenting in this thesis will assume a light source of 1.55 μm which is compatible with the wavelength of peak Er emission.

Note that while the peak emission of Er in silicon is at 1.54 μm [3-5], a lot of work on modulators has been done at wavelengths of 1.55 μm [6, 14 and 15], because it is the wavelength of minimum absorption in silica fibre optics. In order to keep this work consistent with literature data, a wavelength of 1.55 μm is used in the simulations of the waveguides and the modulator. This discrepancy is not significant, since this is a small difference and the waveguide and modulator designs presented here should work at 1.54 μm with minor modifications.

Most work in the literature on silicon based waveguides has focussed on multimode waveguide analysis [11, 14], although Soref et al. has published analysis on single mode rib waveguides [12]. The advantage of single mode waveguides are that they are subject to

lower dispersion losses and they lend themselves to more efficient modulator designs (phase change instead of amplitude change modulation schemes). The disadvantage of single mode fibres is that, in general, their core sizes tend to be smaller than those of multimode waveguides, which makes their end-to-end coupling to optical fibres and other optoelectronic devices, like sources and detectors, more inefficient. The present work presents some analyses of single mode waveguides and examines several issues such as losses to the substrate, losses to metal contacts and bending losses which are important considerations in the design and fabrication of waveguides.

2.2 Free Carrier Effect

Electro-optic modulators on silicon are usually based on the free carrier effect in which free carriers (electrons or holes) are injected into silicon to modulate light [6-16]. This effect is based on the fact the free carriers change both the real part of the refractive index, n and the imaginary part or the absorption coefficient, α, of silicon, which can, in turn, be used to modulate light [6]. See figure 2.1 and figure 2.2.

Free carrier refraction and absorption are caused by the fact that free carriers change the complex permittivity of silicon, ε_{Si}. As a result, the index of refraction n, may be considered to be replaced by a complex index, $n'-j\alpha$, since the index of refraction is given by the square-root of the relative permittivity. The negative sign is consistent with the convention where the phase advance of a wave is given by exp(-jkz) [35].

Although free carrier refraction changes the phase of a mode by changing the real part of the index of refraction, $\Delta n= n-n'$, and does not directly change the intensity of the guided mode, it can be used to change the intensity of light in a number of different ways. For example, the Mach Zehnder set up as described in Haus et al. [35] uses constructive and destructive interference to cause intensity changes. A modulator based on Fabry-Perot

cavities has also been proposed [15]. In this case, changing the real index of refraction changes the resonance length of the cavity, which changes the output intensity of the modulator. The modulation scheme that will be described here is mode coupling, which I will describe in the next section. Modulators, which are based on the free carrier refraction, require single mode waveguides. On the other hand, the free carrier absorption effect, α, changes the intensity of the light directly and does not require single mode waveguides. This effect is less efficient than the free carrier refraction effect.

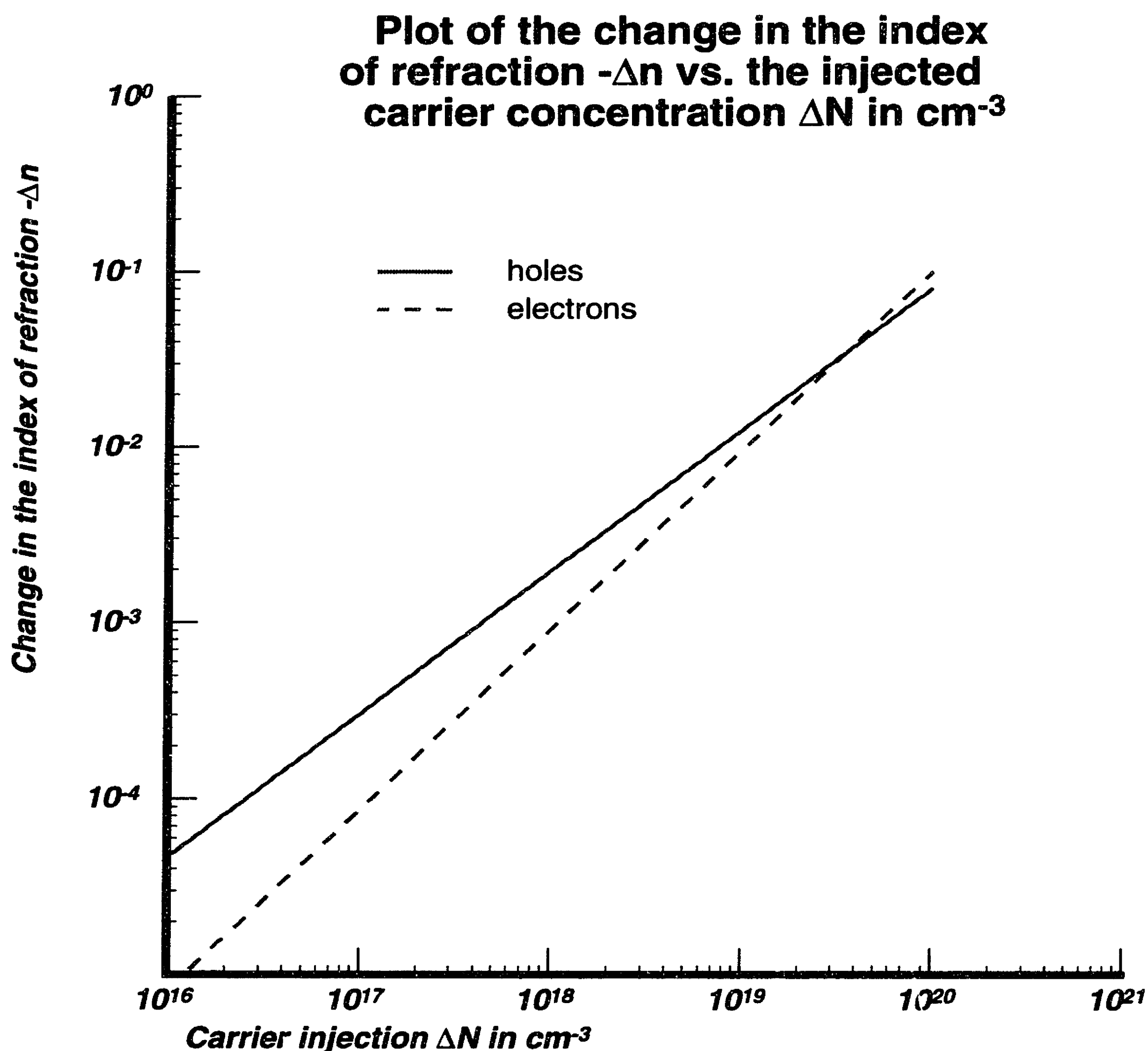

Figure 2.1: Graph showing the free carrier refraction effect at λ=1.55 μm (from reference.[6])

The free carrier refraction effect will be used in the modulator presented here. In fact, the free carrier absorption effect will be suppressed as much as possible to minimize losses, since waveguide coupling only requires a change in the real part of the index, as will be shown in the next section. At λ=1.55 µm, the equations relating the change in the real index of refraction, Δn to the electron and hole concentrations, ΔN_e and ΔN_h respectively are given by [6]:

$$\Delta n = -3.499 \times 10^{-21} \cdot (\Delta N_e)^{1.0228} \quad (2.1)$$

and

$$\Delta n = -5.369 \times 10^{-18} \cdot (\Delta N_h)^{0.80866} \quad (2.2)$$

As can be seen from figure 2.1, the change in index due to the injection of holes is larger than that of electrons. To get a reasonable index change of $\Delta n=-10^{-3}$, the injected hole concentration should be about $10^{18}cm^{-3}$. At this level of injection, the coefficient of attenuation α, is 5 cm^{-1}, which corresponds to a loss of approximately 20 dB/cm. Hence, if a device, like a phase shift modulator, uses the free carrier effect, it should be about 500 µm in length or less, to get a reasonable loss of less than 1 dB. On the other hand, if the device is based on the free carrier absorption effect, the device length will have to be about 1 cm long to get a reasonable modulation depth.

Figure 2.2 also shows that if the doping concentration of a single crystal silicon substrate is low, then the absorption coefficient of the substrate is negligible. For example, if the substrate doping is $10^{16}cm^{-3}$ or less, the absorption loss is on the order of 0.1 dB/cm. Thus, in all loss simulations presented here, the losses due to substrate doping was neglected.

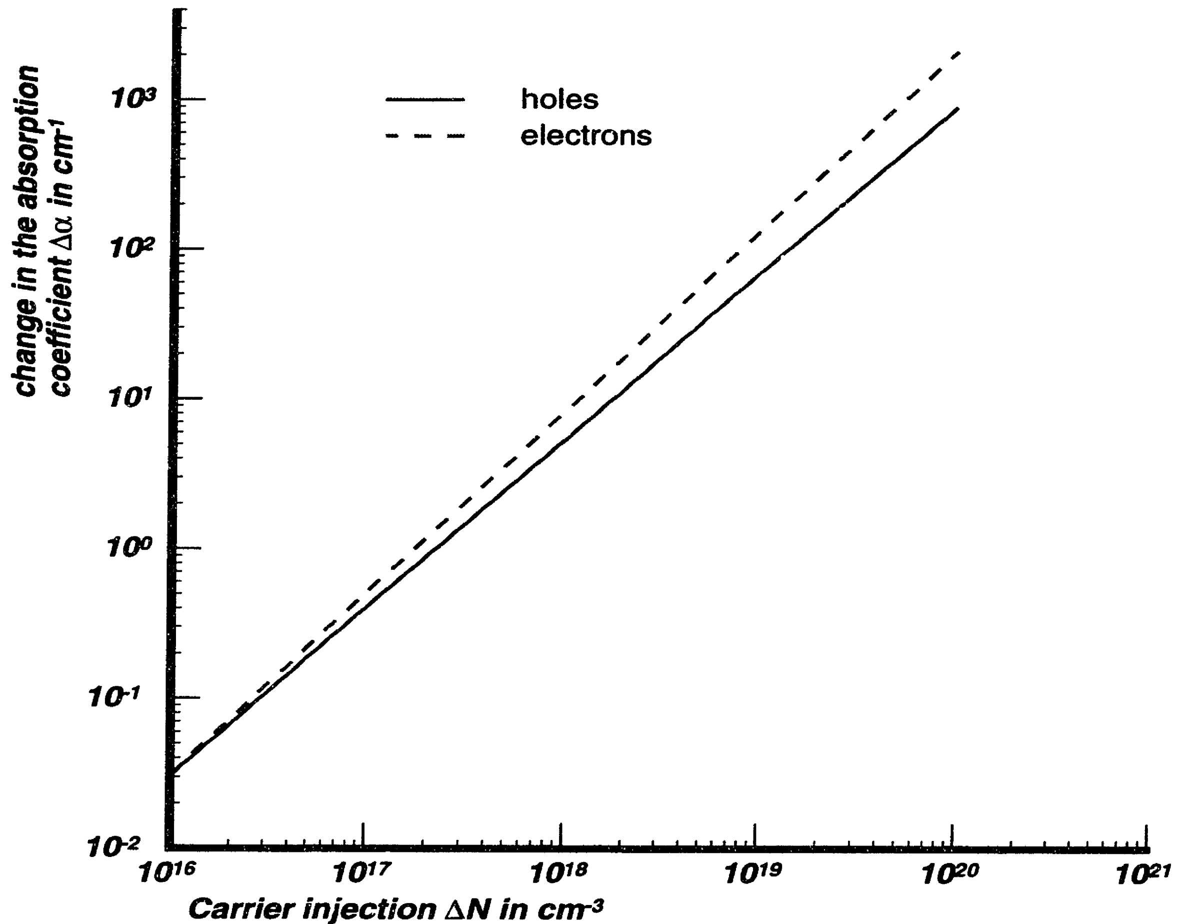

Figure 2.2: Graph showing free carrier absorption effect at λ=1.55 μm (from reference [6])

The low absorption loss for lightly doped single crystalline silicon is the reason why most silicon based optical devices are based on single crystalline silicon instead of polysilicon silicon. The corresponding absorption losses for amorphous silicon and CVD deposited polycrystalline silicon films are on the order of 1000 dB/cm and 10-1000 dB /cm respectively [9], due to the large number of dangling bonds and trapped charges in these materials [8]. In addition to absorption losses, scattering losses due to the grain boundaries in polycrystalline silicon may be large. Finally, using the free carrier refraction effect in

polysilicon will be a difficult task, since it is hard to inject large amounts of free carriers into polysilicon due to the presence of grain boundaries. This makes single crystal silicon the material of choice for waveguides at this moment, although there is still considerable interest in developing polysilicon waveguide technology, since polysilicon on oxide waveguides will be much easier to fabricate than single crystal silicon on oxide waveguides [10] (See section 3.4.6).

2.3 Injection Mechanism

Since the free carrier effect relies on carrier injection, this effect is rate limited by carrier generation and recombination velocities. These effects are unfortunately relatively slow when compared with the Pockels effect, in which the change in the index of refraction of the material results from the application of an electric field. As a result of the need to use to the free carrier effect, the maximum theoretical switching speed of silicon electro-optic modulators will be limited to about 10's Ghz.

MOS [14] and p-i-n based [11, 16] structures have both been proposed in the literature as devices which could potentially be used to inject free carriers. The device which will be used for injecting carriers in this report, will be based on a p-i-n diode. This structure has several advantages, including the minimization of carriers in the guided mode region when the diode is in the off state, which in turn minimizes free carrier absorption of the fundamental mode. Moreover, the theoretical limit in switching speed for these devices are quite high, on the order of GHz [39]. The downside to this device is its large current drive and power requirements, since it will be in the high level injection limit, when the diode is in forward active.

2.4 Dielectric Coupling Modulators

The modulator that I will be designing will be based on waveguide coupling. It is well known that if two waveguides are placed in close proximity, the modes of the two waveguides will couple. If energy propagates down one of the two waveguides, it will couple into or “enter” the other guide as a result of the mode coupling. See figure 2.3. If the two waveguides are identical, the energy from the first guide will couple completely into the second and back to the first. The coupling length is defined as the length over which there is maximum power transfer from in one waveguide to the other.

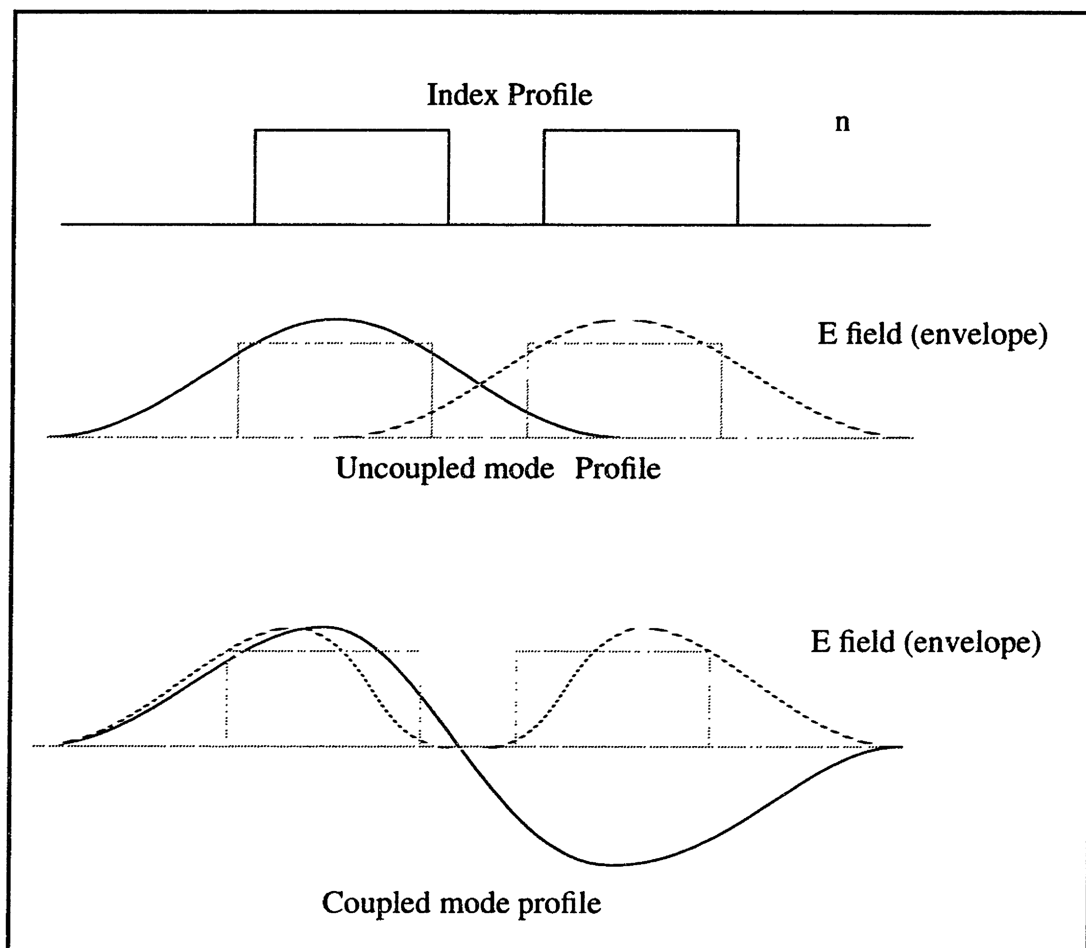

Figure 2.3: Cross sectional view of the generalized index profile and field pattern

Electro-optic modulation in a coupling device is brought about by one of two mechanisms or a combination of both. In the first mechanism, the change of the index of refraction of one of the waveguides modifies the difference in propagation constants of the two lowest modes of the waveguide coupler. If the coupling length is carefully adjusted in both the on and off states, the energy can be forced to remain in or couple back into the input guide. The second method involves changing the propagation constant of one of the waveguides enough so that there is no phase matching between the waveguides. This reduces magnitude of the power exchange between the two waveguides. The first mechanism of modulation is dominant for small core index changes with respect to the difference between the core and cladding indices, while the second requires a relatively large change in the index of the core with respect to the cladding index. See figure 2.4.

The coupling equation for waveguide I is given in [35] by:

$$\frac{da_1}{dz} = -j\beta_1 a_1 + \kappa_{12} a_2 \tag{2.3}$$

where the subscript 1 and 2 refer to waveguides I and II respectively and a_1 is the amplitude in guide I. As the system is reciprocal, an analogous equation can be written for guide II. The solution to these two equations yields 2 eigenmodes which have different propagation constants, given by

$$\beta = \beta_1 + \beta_2 \pm \sqrt{\left(\frac{\beta_1 - \beta_2}{2}\right)^2 + |\kappa_{12}|^2} \tag{2.4}$$

The two eigenmodes are shown in figure 2.3. Changing the index of refraction not only changes the propagation constants of both eigenmodes, it also changes the relative magnitude of the eigenmode in each of the waveguides. The first effect changes the cou-

pling length of the waveguide coupler, while the second effect changes the coupling efficiency of the modulator.

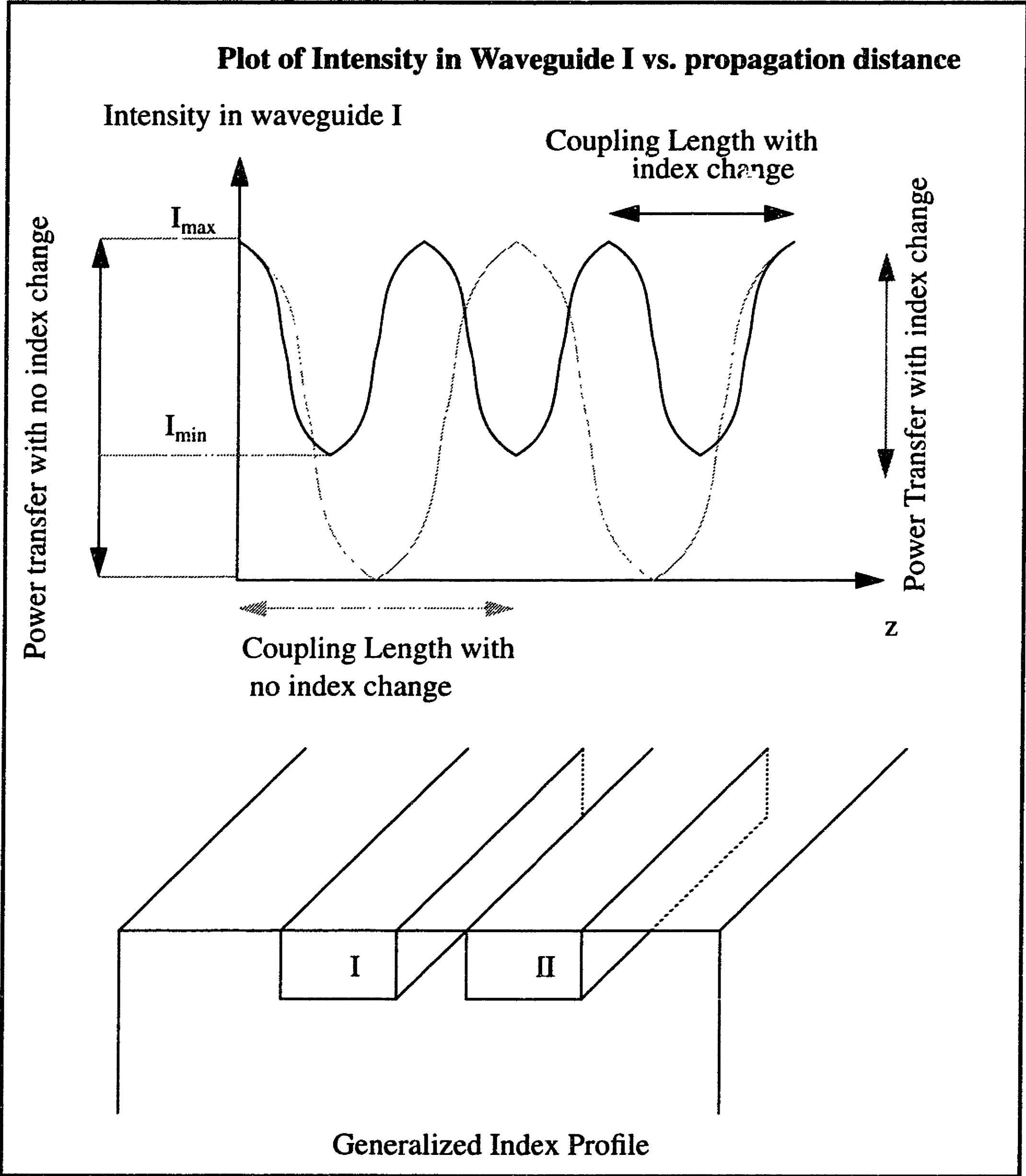

Figure 2.4: Schematic showing waveguide coupling

The coupling constant κ_{12} is given by:

$$\kappa_{ij} = -\frac{jw}{4}\int d\sigma\delta\varepsilon E_i \cdot E_j^* \tag{2.5}$$

where the integral of the product of the electric fields E_j and E_i and the perturbed dielectric index of refraction $\delta\varepsilon$ is taken over the cross sectional area of the perturbed index.

As can be seen from equation (2.5), the strength of the coupling constant will depend on the magnitude of the evanescent E field due to the 1st guide overlapping with the 2nd guide. Thus from this analysis, one may conclude that coupling modulators are best built with a waveguide system in which a significant amount of the E field is evanescent, or outside the high index core of the waveguide. The most important geometrical quantity is the waveguide separation, as the coupling length varies exponentially with waveguide separation. The reason for this is that the evanescent fields decay exponentially outside the core of the waveguide. As a result, the waveguide separation has to be built to extremely tight tolerances.

Waveguide coupling modulators are especially useful for modulation of light in silicon since, unlike most phase shift modulators, these modulators does not require spatial coherence, which eases the restrictions on the source. Although these modulators tend to be less efficient than phase modulators in terms of modulator length for a given level of carrier injection density, this technology may be compatible with the Er based silicon LEDs that have been fabricated recently [2] and does not require the use of integrated circuit lasers. On the other hand, there are issues which will have to be resolved if LEDs are to be used as light sources, for example, the coupling efficiency of the light from the LED into waveguide has to be maximized.

Modulators of this type can only modulate one mode at a time, since the coupling length of the modulator is dependent on the propagation constant of the guided mode. In order to achieve efficient modulation, the input waveguides must be single mode, so that when the two waveguides are placed in close proximity only the two lowest modes are

excited. Hence, all the waveguide structures that will be considered in the next section will be single mode waveguides.

2.5 Simulations and Calculations

2.5.1 Waveguide and Eigenmode Simulations

The waveguide and modulator structures were simulated using a simulator based on the finite difference beam propagation method [19]. This method was developed at the University of Waterloo by Huang et al. and solves the paraxial wave equation by finite difference calculations. It is necessary to use simulations to refine the waveguide structures because there is no accurate analytical method of studying general 2 dimensional waveguides. The simulator was used in calculating the eigenmode profiles, as well as in simulating both propagation and loss in waveguides and couplers.

In order to simulate the eigenmode, an imaginary distance propagation method was used with the aforementioned simulator [20]. To simulate the loss of the guided mode, the eigenmode of a lossless structure was first determined (e.g. without the substrate) and used as the input to the lossy structure (e.g. with the substrate). The amplitude of the mode in the guide was then calculated and the loss in dB was determined.

To simulate coupling, the eigenmode of one of the waveguides is first determined and is used as the input to waveguide I. The energy is then propagated down the structure and the resulting fields were plotted and analyzed. See figure 2.4.

In all optical beam propagation simulations, a value of 3.48 was used for the refractive index of silicon. [7]

2.5.2 Waveguide Bending Loss Calculations and Simulations

In order to simulate bending losses, the beam propagation simulator was modified to handle curved waveguides. A lot of simulation work on bending losses in the literature has

focussed on a conformal mapping which transforms the index profile of a curved waveguide with a constant radius of curvature to an index profile of straight waveguide. The transformed straight waveguide would have an index profile which would yield the correct bending loss, if the propagation problem is solved. The propagation of a field distribution applied to this index profile can be simulated by using a beam propagation algorithm. The losses of the field can be extracted. This analysis was developed by Heiblum et al. [23] and was implemented by Baets et al. [25] and it has the advantage of avoiding discretization errors that the full z dependent simulations would have.

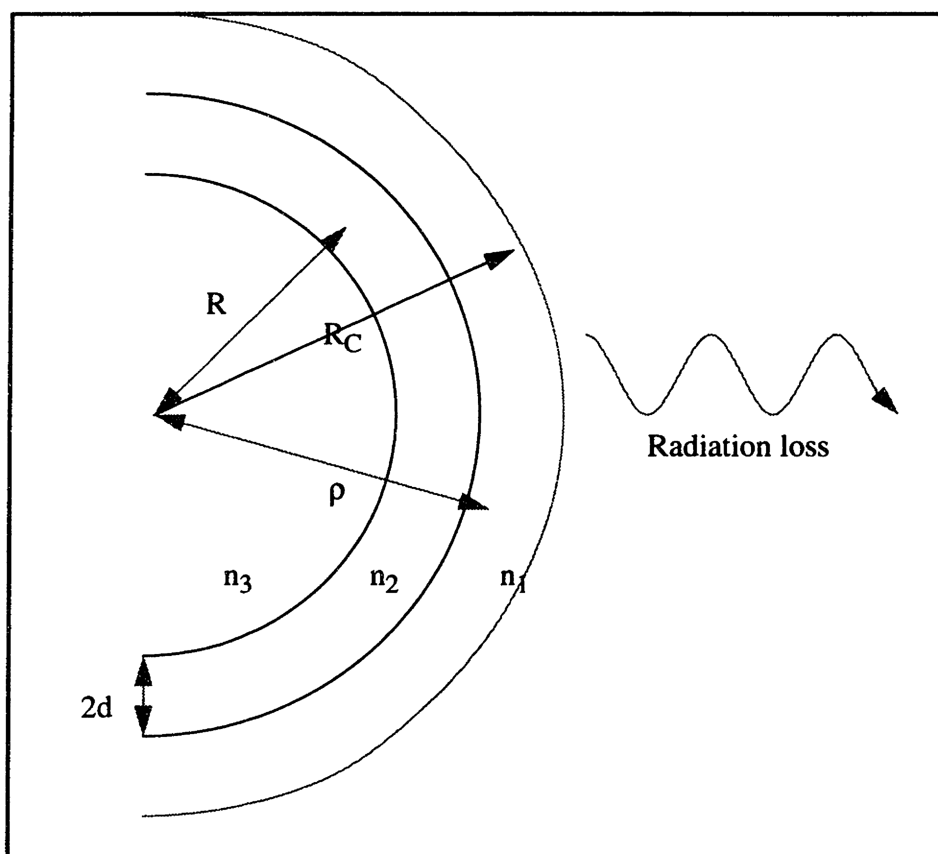

Figure 2.5: Schematic of radiation loss due to waveguide bending

The conformal map involves a standard log transformation:

$$W = R \times \ln(\frac{Z}{R}) \tag{2.6}$$

The net result of this conformal map is a transformation of the index at any point n(x,y) such that:

$$n'(x, y) \rightarrow n(x, y)\ (1 + \frac{\rho}{R}) \tag{2.7}$$

where ρ is the distance of the point to the center of curvature. See figure 2.5. In this figure, $n_2 > n_1$ and n_3. Thus the field is confined largely to the material with index n_2. This transformation holds true for large values of ρ, such that $\rho >> 2d$. When this restriction is satisfied, there is no transformation of the x coordinate.

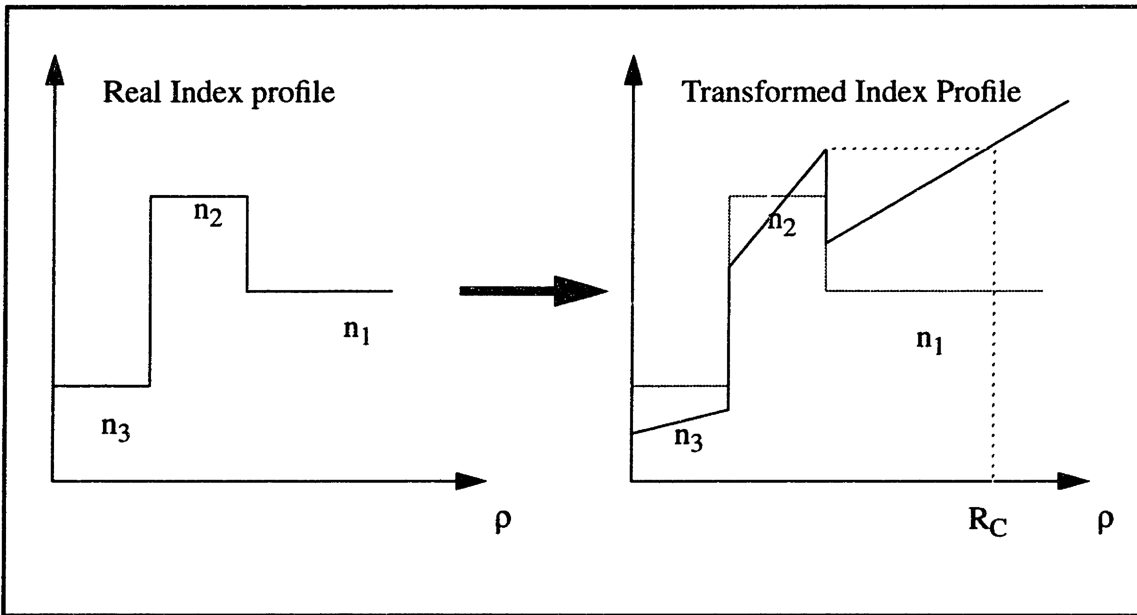

Figure 2.6: Schematic of conformal map as proposed by Heiblum et.al. [23]

A schematic for the transformation is shown in figure 2.6. As is apparent from the schematic, the transformed index of refraction of the material with index n_1 will increase to a point $\rho > R_C$, such that the value $n_1(1+\rho/R)$ is more than n_2, for $R > R_C$. Thus, the field which is originally in n_2, will leave the core to move into this region of higher index. As

the radius of curvature increases, R_C increases linearly, resulting in an exponentially decreasing power loss due to bending.

In order to test the bending loss algorithm in the simulator, simulations were run and compared with analytical computations, which have been published in the literature. The simulator was used to predict GaAs/AlGaAs rib waveguide bending losses and the results were compared to measured bending losses that have been published in the literature. I will discuss the analytical solution here, but will leave the results of the GaAs/AlGaAs rib waveguide analysis to section 3.3.4.

Marcatili first solved approximately the fields in the slab waveguides and showed that waveguides radiate power if they are bent [22]. Marcuse used a perturbation method to solve the bending loss problem [21] and showed that his results were numerically similar to those obtained by Marcatili. Lee used a simplified method similar to Marcuse's to solve the problem with the effective index method [33]. Marcuse's method will be presented here.

The equation for the loss coefficient alpha (in cm^{-1}) as derived by Marcuse is:

$$\alpha = \frac{2\gamma\kappa^2 e^{2\gamma d} e^{-U}}{(n_2^2 - n_1^2)\,k^2\beta\,(2d + \frac{1}{\gamma} + \frac{1}{\theta})} \tag{2.8}$$

where

$$U \approx \frac{2}{3}\frac{\gamma^2}{\beta^2}\gamma R \tag{2.9}$$

and

$$\beta = \text{propagation constant}$$
$$2d = \text{slab width}$$
$$\kappa = \sqrt{n_2^2 k^2 - \beta^2}$$
$$\gamma = \sqrt{\beta^2 - n_1^2 k^2} \tag{2.10}$$
$$\theta = \sqrt{\beta^2 - n_3^2 k^2}$$
$$k = \frac{2\pi}{\lambda}$$

The approximations are valid if the following inequalities are satisfied

$$\beta < n_2 k \left(1 - \frac{d}{R}\right)$$
$$\beta > n_1 k \left(1 + \frac{d}{R}\right) \tag{2.11}$$

The reason why bent waveguides radiate power is that there is a phase mismatch between the E field in the core and that in the cladding. Thus the outer cladding is unable to support the required E field at the velocity of propagation and power is radiated from the core. Since the radiation loss occurs from the cladding it is obvious that in waveguide systems where the radiation is confined largely in the core, the bending losses will be negligible and vice versa for waveguide systems in which a large fraction of the E field is evanescent or outside the guide.

Note that the losses calculated here are only approximate and that they were derived for the strip waveguide described in section 3.4.

2.5.3 Process and Electrical Simulations

The AT &T process simulator PROPHET and device simulator PADRE was used to simulate the electrical characteristics of the device. PROPHET was used to model a possi-

ble fabrication process flow for the modulator which was designed with the aforementioned beam propagation simulator. The output of PROPHET is a dopant distribution which was used as an input to PADRE so that the electrical characteristics of the device can be simulated.

Chapter 3

Waveguide Design

3.1 Waveguide Structures

The design of a modulator is strongly dependent on the design of the waveguide and vice versa. Furthermore, in order to design an efficient modulator, the waveguide structure on which it is based must first be optimized. I am restricting my analysis to single mode Si based waveguides, since coupling modulators require single mode waveguides. There have been several structures that have been proposed, of which I will consider 2:

• Si core with a SiO_2 and air cladding on a silicon substrate which is also known as strip or slab waveguide.The cross sectional view of a strip waveguide is shown in Figure 3.1. The mode is guided in the silicon core with SiO_2 and air as the cladding. This entire structure is on a silicon substrate.

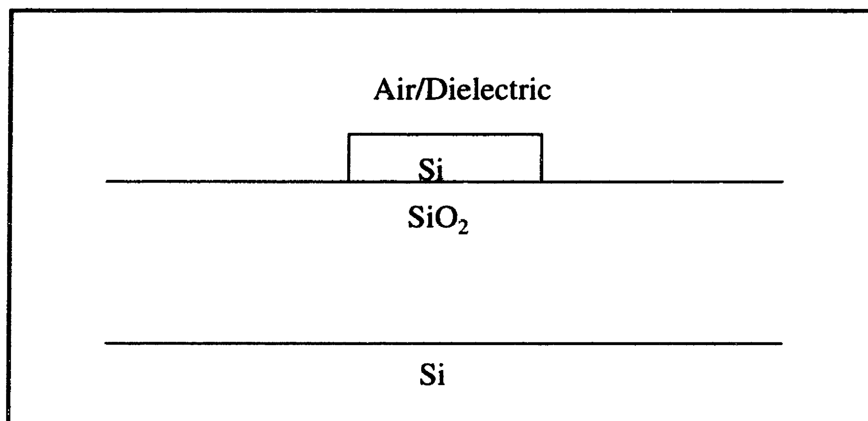

Figure 3.1: Schematic of a strip waveguide

• Si core with a SiO_2, Si and air cladding on a silicon substrate, also known as a rib waveguide. The cross sectional view of the rib waveguide is shown in figure 3.1. It is convenient define the dimensions of the rib waveguide structure with respect to the wavelength of the light. The ratio of the width of the structure to wavelength is 2a and the ratio

of the height of the structure to the wavelength is 2b. In the rib waveguide, the core region is the tall central region shown shaded while the surrounding Air/Si/SiO_2 stack is the cladding. This cladding stack has an effective index which is less than, although very close to the effective index of the core stack. This difference in index results in guiding. The strip waveguide is in fact a special case of the rib waveguide with r=0.

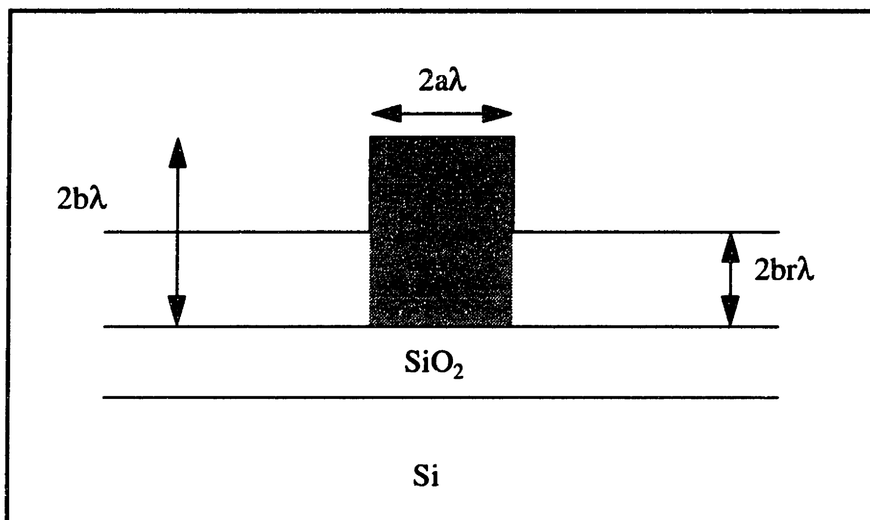

Figure 3.2: Schematic of the rib waveguide

- A third waveguide structure which is under consideration is that of a Si-Ge core with a silicon/air cladding

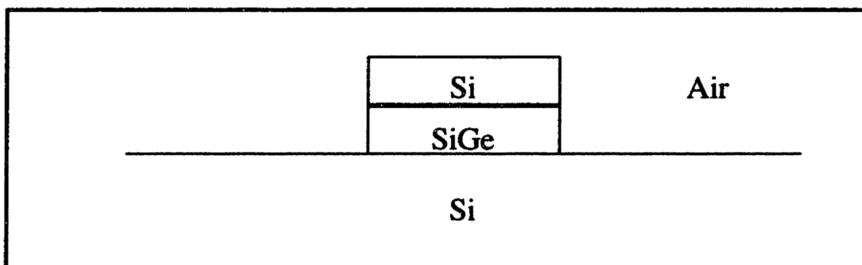

Figure 3.3: Schematic of the Si-Ge waveguide

Silicon-germanium affords several advantages. Firstly, silicon on oxide technology (SOI) is not required. In addition, Si/Si-Ge heterostructures can be used in optical detectors and in LEDs which may make it worthwhile to study SiGe based waveguides. This material

system does however, bring with it its own processing problems.

There are other single-mode silicon waveguide schemes, such as the ARROW technology proposed by Soref et al. [13]. These structures are like the rib waveguides, in that they are relatively large and their single-mode nature is derived from having the higher order modes leak out of the central core region. However, due to the lack of time, only the first two structures were evaluated in this report.

3.2 Design Considerations

3.2.1 Strongly Confined vs. Weakly Confined Waveguides

In designing coupling modulators, it is convenient to classify the waveguides, on which they are based, into one of two types:

- "strongly confined" where the index of the core is significantly larger than the cladding e.g. Si core with air and/or SiO_2 cladding.
- "weakly confined" where the index of core is similar to that of the cladding e.g. Si/Ge core with Si cladding.

Although the rib waveguide has a silicon core, it is "loosely confined" in the direction parallel to the surface of the substrate, since the effective index of its cladding (the Air /Si structure) is similar to that of the core.

Coupling modulators are most efficiently built around "weakly confined" waveguides, since the evanescent fields of weakly confined waveguides are larger than those of strongly confined waveguides of the same dimensions. In addition, loosely confined waveguides have larger single mode cutoff dimensions than those of strongly confined waveguides.

However, for the minimization of bending losses, that is, losses associated with waveguides that are curved, "strongly confined" waveguides are optimal, see figure 3.6.

Bending losses are a result of mismatched phase between the evanescent field and the eigenmode in the core since the path length in the core and around the cladding for a waveguide of finite width is different. See section 2.5.2. We know intuitively that this must be the case since strongly confined waveguides have smaller critical angles than those of weakly confined guides. Thus the strongly confined guides can tolerate much more bending than weakly confined guides for similar kinds of loss. This irreconcilable requirement is one of the fundamental problems of waveguide couplers and a trade off must be made when fabricating these devices.

3.2.2 Waveguide Losses

There are several ways in which waveguides may be lossy and it is convenient to consider identify losses as one of two types:

- radiation losses, which I will define as losses which are intrinsic to the design of the waveguide, e.g. bending losses, and
- scattering losses, which I will define as losses which are extrinsic to the design, e.g. losses due to process variation.

Intrinsic radiation losses include losses to the substrate and to the metal contacts, if any. Loss to the substrate is a potential problem in rib and strip waveguides based on the Si/ SiO_2/Si/air stack. The reason is that the mode in the Si core will "couple into the substrate" through the dielectric SiO_2. In addition, there can be significant losses to metal contacts, if present, since the frequency of the light is below the plasma frequency of the metals. Thus, the loss due to absorption by the metal will be large. These metal contacts are necessary because the modulator operates on hole/electron injection, which requires the use of a contacted electronic device like the p-i-n diode. In order to alleviate this problem, an MOS device operating in the depletion mode may be proposed as an alternative [17].

An MOS structure would have lower contacting losses, since some of the evanescent fields would reside in the oxide. If the oxide is thick enough, the magnitude of the evanescent field inside the silicon core will be reduced to a point where the losses to the metal contact will be minimized. The problem with such a device is that it is hard to get a high levels of charge in and out of the silicon core rapidly. In addition, an additional contact to the silicon core is still necessary since the Si core has to be grounded.

Another contacting scheme would be applicable to SiGe/Si heterostructures. Here the high index SiGe would serve as a waveguide core as well as a potential well in which carriers reside. As a result the contacts can be made some distance away from the SiGe layer, which would ensure minimal losses due to interaction of the E field with the contacts.

One of the main causes of scattering losses will be due to surface roughness of the waveguide. The scattering loss due to surface roughness of a given spatial frequency, ω, can be described by a loss coefficient, $\alpha(\omega)$, as derived by Ames et al. in [24]. It is given by:

$$\alpha(\omega) \propto \int_A \Delta n^2 E^2 g(\omega)\, dA \tag{3.1}$$

where, A is the area over which the surface roughness occurs, E is the electric field at the interface and Δn is the index difference at the rough surface of the waveguide. From the equation, the losses due to scattering are strongly dependent on the E field and the index difference between the core on the cladding. Hence, to minimize losses, the E field at the core/cladding interface must be minimized and the index of refraction difference between the core and cladding should be reduced.

Although such surface roughness is inevitable due to the reactive ion etch (RIE) which is required to form the vertical sidewall, the roughness must be minimized to ensure that scattering losses remain tractable. A paper by Seto et al. shows that a large part of bending

losses which have been attributed to radiation due to bends is in effect due to scattering losses in bent waveguides [27]. Some of this roughness is due to the finite surface roughness as a result of lithography writing schemes. Another source roughness is the RIE techniques to create vertical side walls. Seto showed that by using wet, diffusion limited chemical etches, the waveguides surfaces are smooth, although not vertical. The problem with this is that ribs with non vertical sidewalls have poorer confinement than those with vertical walls [26]. In fact it has been shown that scattering losses increase with increasingly sloped sidewalls if the surface roughness stays the same. However, with the proper etch and smoothing procedures surface roughness can be reduced to a minimum and vertical sidewalls should also be achievable.

3.3 Rib Waveguide

3.3.1 Dimensions

The rib waveguide structure has been proposed in the literature [12]. In fact, typical single mode waveguide dimensions for the silicon-air-oxide structures are discussed by Soref et al. and I have used their analysis as a starting point in my simulations. The dimensions for the rib waveguides that are presented in this thesis are as follows: heights of 2-5 μm, with an etch-back of r=0.5, (see figure 3.2) and widths of 1-3 μm. This is consistent with the dimensions suggested in the paper which suggested an r value of not less than 0.5. For the waveguide with dimensions, $2a\lambda = 3$ μm and $2b\lambda = 5$ μm, the a/b value is =0.6 and the waveguide supports only the EH_{00} mode. In fact, these waveguides are scalable and it is possible to design smaller waveguides or larger ones. These dimensions were chosen to make the rib waveguides easy to fabricate and to approximate the size of rib which would be required to couple to optical fibres [12].

The rib waveguide works by allowing all but the fundamental mode in the large rib section to be supported by the Si/air "cladding" surrounding the large rib section. Thus the higher order modes will leak out of the center section into the cladding section leaving only the fundamental mode in the core. According to Soref et al., this mode leakage will occur over a length of several mm before the eigenmode stabilizes. This setup results in relatively large waveguide dimensions.

3.3.2 Eigenmode Simulations

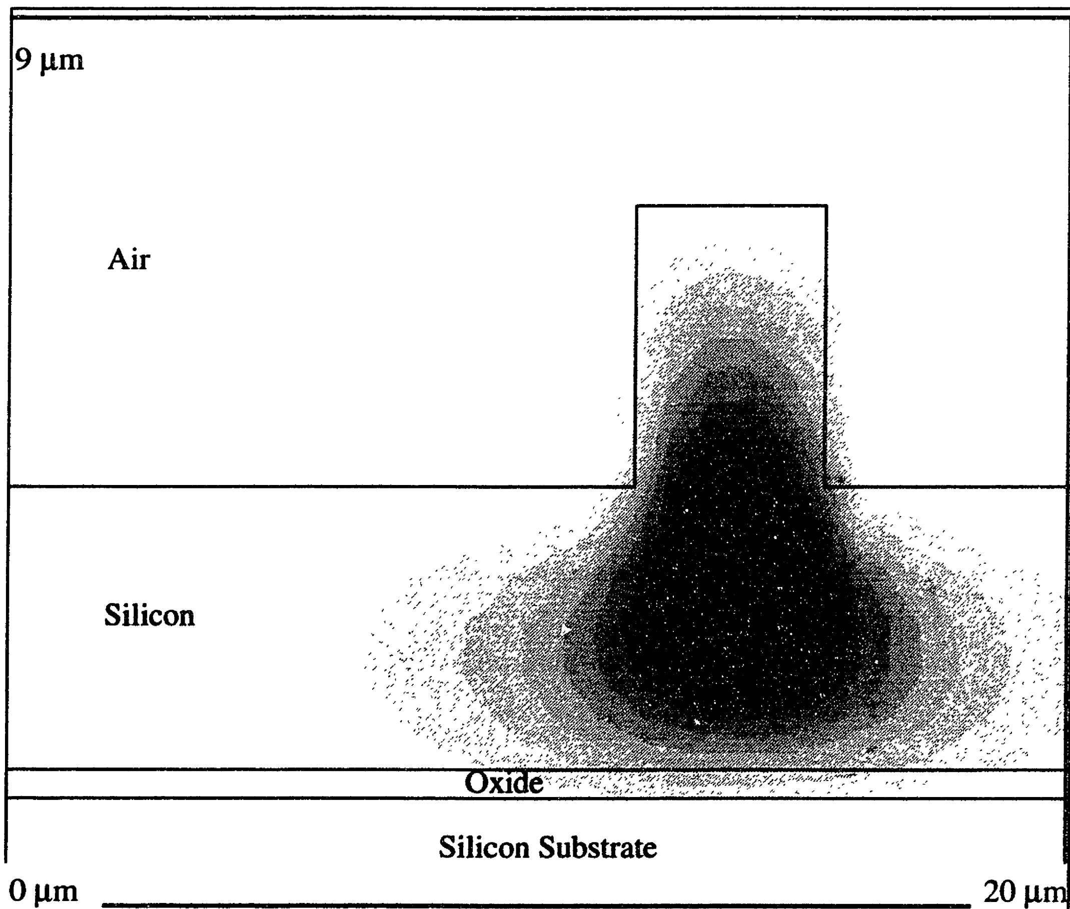

Figure 3.4: Cross section of a rib waveguide of dimensions 3 μm by 5 μm, r=0.5 and eigenmode of the guided mode. (Simulation of 140x90 points, scale 10pts:1 μm)

The eigenmode of the rib waveguide is shown in figure 3.4. The electric field, as is expected, is concentrated in the rib section and does not extend much into the SiO_2 or air. This fact is not surprising, since the silicon core is extremely large and the index change from the silicon core to the Air and SiO_2 is large. Hence, most of the field is strongly confined in the silicon. This fact is shown to be of importance in loss simulations.

On the other hand, the E field "leaks" significantly beyond the width of the rib section into the surrounding silicon. This leakage of E field is a result of weak confinement parallel to the silicon substrate. As mentioned earlier in section 2.4, this is the most efficient configuration for waveguide coupling.

3.3.3 Loss to Substrate Simulations

In the rib waveguide structure, the loss to the substrate is minimal since the waveguide height is large and the vertical extent of the E field is confined the silicon core. In addition, the E field is strongly confined in the direction perpendicular to the silicon substrate. Therefore the coupling coefficient between the core and the substrate is extremely small. For example, the loss to substrate of the 3 μm x 5 μm waveguide is less than 0.3 dB/cm.

Note that as the waveguide dimensions are reduced, the magnitude of the evanescent field increases, which results in larger losses to substrate. The reverse is true as the waveguide sizes are increased.

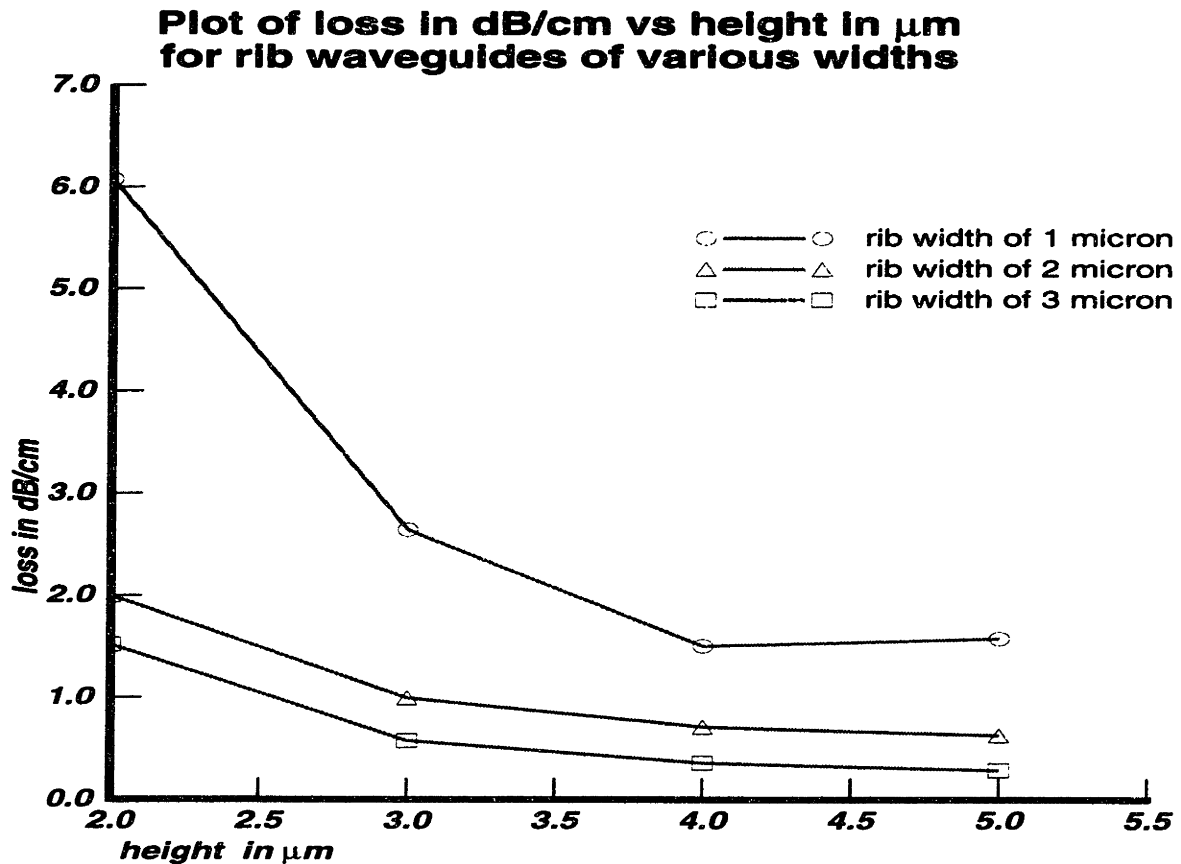

Figure 3.5: Simulation of loss to substrate in rib waveguides for heights between 2 µm & 5 µm and widths between 1 µm & 3 µm (r=0.5; oxide thickness =0.2 µm).

3.3.4 Bending Loss Simulations

As mentioned previously calculations for bending losses of the rib waveguide were attempted using the treatment presented by Marcuse [21] and by using the beam propagation simulator (See section 2.5.2).

Only the 3 µm by 5 µm rib waveguide was simulated with the beam propagation simulator. The results of the bending losses from the beam propagation simulator yields a bending loss of 11.8 dB/cm or less than 0.5 dB/90° bend at a radius of curvature of 100 µm. The corresponding value for a radius of curvature of 300 µm is 1 dB/cm.

The result of the Marcuse calculation is plotted in figure 3.6. As can be seen from the graph, the bending losses for a 3 micron x 5 micron waveguide is extremely large. The radius of curvature of the waveguide has to be about 7 mm for losses of less than 1dB/cm. The radius of curvature of a given amount of loss differs by more than an order of magnitude between the 2 methods.

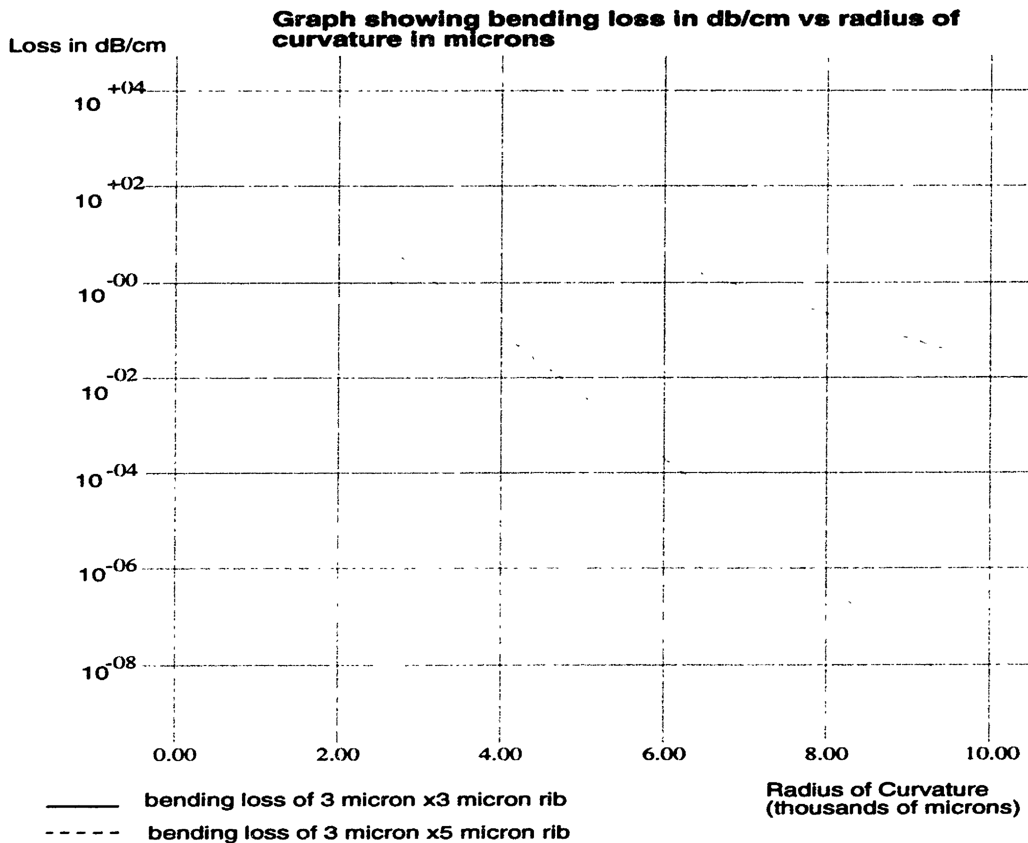

Figure 3.6: Bending loss in dB/cm for rib waveguides of various dimensions vs. bending radius in μm using Marcuse's approximation. See text.

In order to put this data into perspective, both the beam propagation simulation and Marcuse's analysis were applied to AlGaAs/GaAs rib waveguides which have been studied in the literature by Seto et al. and Austin [27-28]. I found that Marcuse's analysis overestimated the required radii of curvature for 1dB/cm bending losses by almost an order of

magnitude. The reason for this large discrepancy is that the field distribution for a slab waveguide is quite different from that of the rib waveguide. Unfortunately, as was mentioned in section 2.5.2, Marcuse's analysis was derived for slab waveguides since he had to assume field distribution for a slab waveguide. Furthermore, the indices n_1, n_2 and n_3 were extracted by effective index methods. This method is accurate for extracting propagation constants, but is poor when field distributions are important. Obviously Marcuse's analysis in its original form is inadequate for describing losses in rib waveguides.

The results of the simulations turned out to be exactly the opposite from that of Marcuse's analysis -- the loss at a radius of curvature of 100 μm is underestimated by 2 orders of magnitude, 8-12 dB/90° in the literature vs. 0.1 dB/90° simulated. In fact, the simulations indicate that bending losses for radii of more than 50 μm should be negligible, while measured losses are significant up to a radius of curvature of 300 microns. This discrepancy may be due to one of 3 reasons. Firstly, the implementation of the program could be wrong, secondly, there could have been radius dependent scattering losses in the measured guides and thirdly the higher losses could be due to the higher order modes in multimode waveguides.

Although I am unable to rule out the first reason, the second reason may be probable because Seto's data shows that while the losses increase with decreasing radius of curvature, the losses increase differently for different etching solutions. Since each etching solution has its own characteristic smoothness, it may be possible that scattering causes the large increase in loss at small bending radii. At small radii, the gradient of the transformed index increases and the value of R_c decreases. This larger index on the outermost portion of the waveguide core results in a shift of the eigenmode towards the edge of the waveguide core (the n_1 and n_2 interface), which is where all the surface roughness is.

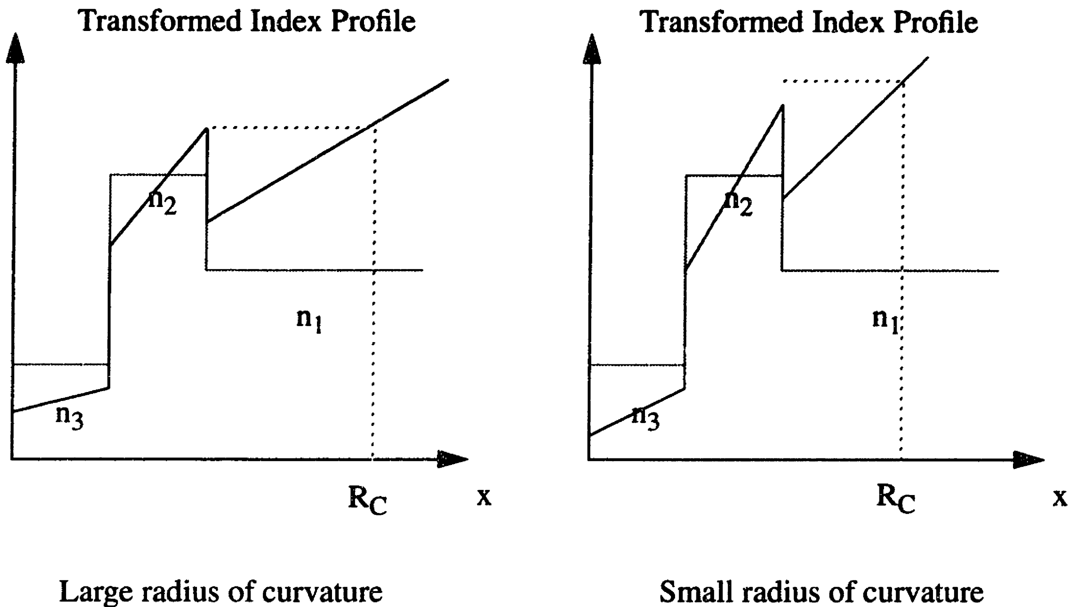

Figure 3.7: Schematic showing how the transformed index profile changes with radius of curvature.

Since scattering losses are proportional to the square of the E field at the rough interface, the scattering losses will increase rapidly with decreasing radius of curvature. This loss is radius of curvature dependent, since it increases with increasing E field at the waveguide surface which in turn increases with decreasing radius of curvature.

There is also imperfect coupling efficiency where the curved waveguide re-joins the straight waveguide. As a result of the index profile change, the eigenmode profile of the curved region will be different from that of the straight part. Thus there will be some loss of power due to the change in eigenmode profile. As the radius of curvature decreases, the mismatch in the eigenmode profiles increase and the coupling efficiency of the eigenmode in the curved section to the eigenmode of the straight decreases. Again this effect is radius of curvature dependent and can explain the losses which is observed by Seto.

Another effect that was neglected in the simulations that could explain the large discrepancy in bending loss between the simulations and the published data, was the effect of having more than one mode in multimode waveguides on the bending. If the waveguides are indeed multimode, the losses would have been much higher than the simulations since the lateral extent of the higher ordered modes is much larger. This makes the higher order modes more susceptible to surface roughness effects. Unfortunately, I was unable to pursue a detailed analysis of these effects as I was short of time.

If bending losses are a problem with the rib waveguides, the problem may be solved by using a three waveguide coupler. Such a coupler will do away with the requirement for bends in the coupler[20]. See figure 3.8.

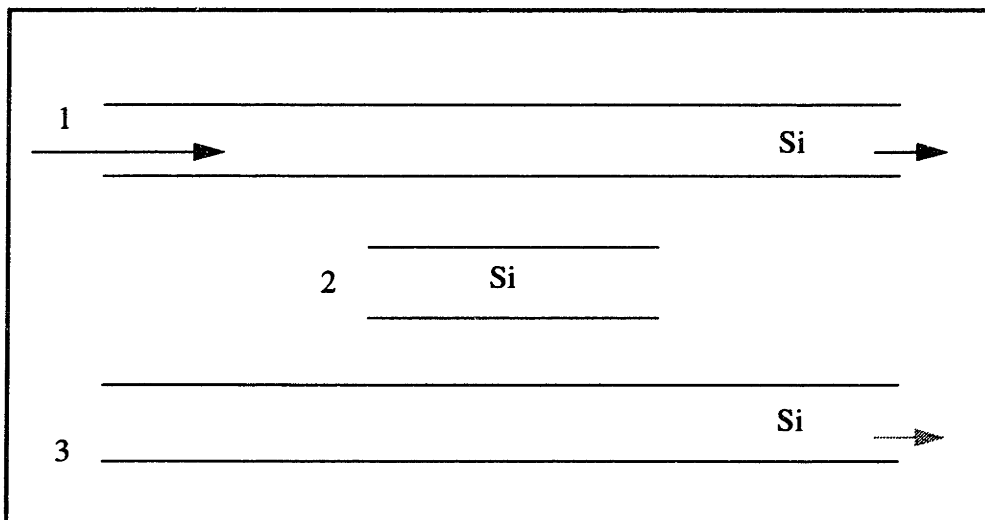

Figure 3.8: Schematic of the three waveguide coupler

The three waveguide coupler works by first having light coupled from waveguide I into waveguides II and III. Eventually, if the structure is symmetric, light will couple into waveguide III. Modulation will again be effected by changing the index of refraction in waveguide II or waveguide III. Light will then be unable to couple from waveguide I into waveguide III and will stay in waveguide I. This structure, therefore does not require

bends to bring the waveguides in from a non-interacting separation, to an interacting separation.

Another way to eliminate bends in general structures would be to use cross couplers (see figure 3.9). These couplers may afford directional changes with lower losses then those of bends and have been developed in Ti:$LiNbO_3$ [30] and InGaAs/InP materials systems [31]. By adjusting the lengths and angle of the waveguides it may be possible to efficiently change the direction of propagation by using mode coupling. In this case light entering waveguide I can be coupled into waveguide II. The change in direction can then be effected by having the waveguides at an angle.

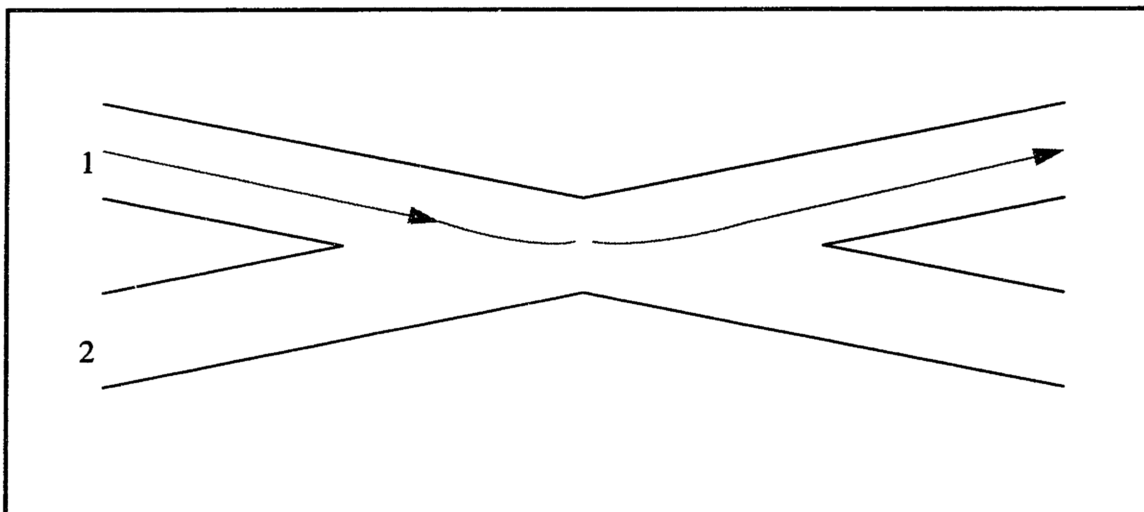

Figure 3.9: Schematic of the cross coupler

3.3.5 Loss to Metal Contact Simulations

In order to determine the losses to the top metal contacts, a simulation was run with a layer of aluminum deposited on the top of the rib of the waveguide. The propagation of an eigenmode which was calculated without the metal was simulated because the eigenmode

simulator could not handle complex indices. The aluminum was modeled with a complex index of n=1.444 + 15.955 j [32].

As is apparent from the figure 3.10, the loss is very small, especially when compared to the loss to the substrate. (See figure 3.5). In fact, the loss is so small that extracting a loss due to the metal contacts will yield figures which are erroneous. The difference in simulated loss between the simulations, with metal and without metal is less than 0.01 dB/cm, which is negligible for this application. The reason why the propagation loss due to the metal contacts is so small is that the E field at the top surface is itself small, due to the large core size and large index change between the silicon and air.

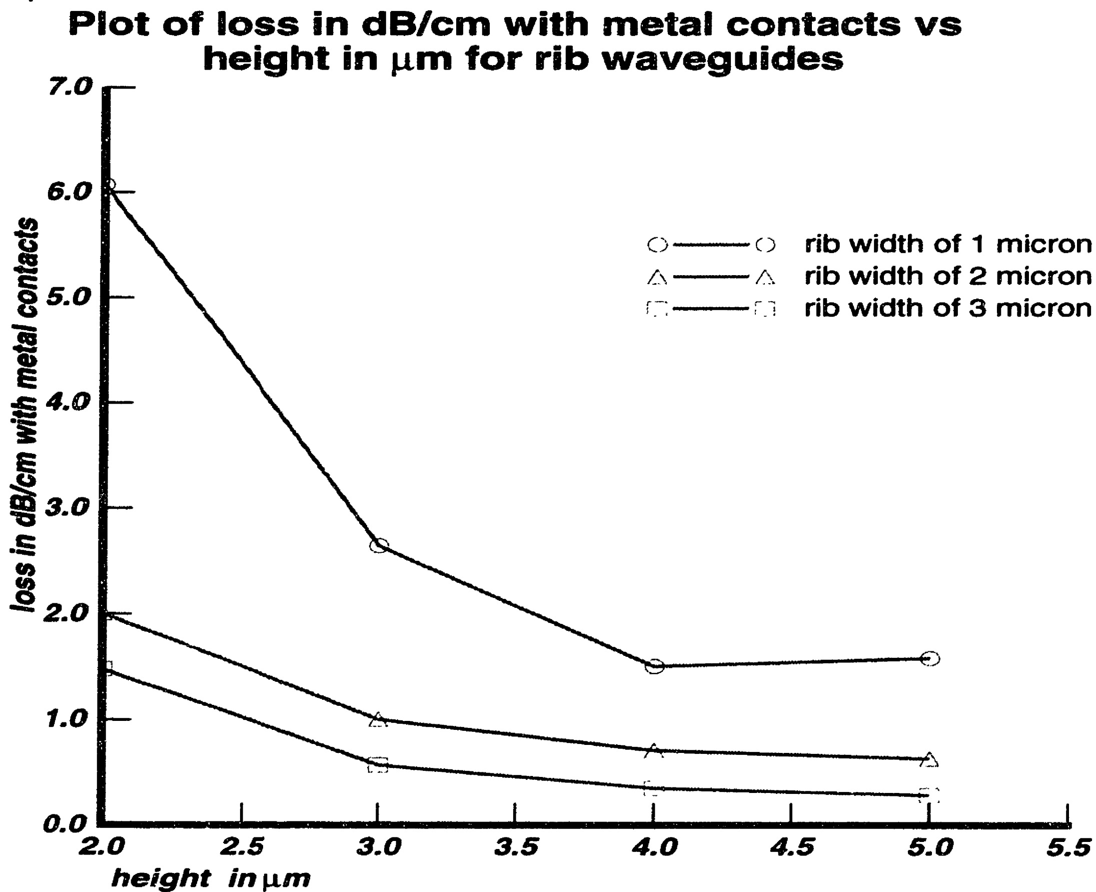

Figure 3.10: Simulation of loss to substrate in rib waveguides for heights between 2 & 5 μm and widths between 1 & 3 μm with top metal contacts (oxide thickness=0.2 μm).

3.3.6 Ease of Fabrication

These structures should be relatively easy to fabricate since the dimensions are on the order of microns. The rib waveguide that I have simulated has a height of 5 µm and width of 3 µm. The loss of the waveguide to substrate with respect to oxide thickness was also simulated. The simulated loss in a rib waveguide is less than 1 dB/cm for oxide thicknesses ranging between 0.2 and 1.0 µm and for waveguide dimensions from 2-3 µm widths and 3-5 µm heights. Thus, a 2000Å oxide may be used since this oxide thickness is compatible with SIMOX material, which simplifies processing.

In a real rib structure, the shelf regions cannot be infinite in extent. The non infinite shelves will change the eigenmode profile of the system and will increase the number of possible modes in the rib. In order to prevent this from occurring, it should be possible to make the shelves lossy by doping the shelves. This will reduce the relative intensity of extraneous modes and will also increase the rate at which an incident E field evolves into the eigenmode of the waveguide. In addition, the shelf should be about 10-12 microns wide so that the first eigenmode will not be "truncated". See figure 3.4.

The rib waveguide is an ideal structure on which to base a waveguide coupling modulator since the lateral extent of the E field into the oxide/Si/air cladding is large. In addition, the structure is relatively easy to fabricate and lends itself to a doping configuration which eases the contacting problems.

The drawback is that the rib waveguide structure tends to be extremely large and this may lead to planarization problem which is necessary for multi-level metallization, although may be alleviated by reducing the size of the rib height. The trade-off that must be considered when reducing the rib dimensions, is that waveguide losses to substrate and to metal contacts increase with decreasing dimensions.

Another problem with the rib waveguide, is the fact that it has to be separated by about 5 μm or 11 μm core separation between the centers of the waveguides to reduce cross talk. This makes the foot print of the rib waveguide extremely large. By extrapolating the coupling lengths which have been extracted in simulations of the rib coupler, (see section 4.1) the coupling length of rib waveguides with a waveguide gap of 5μm (or 11 μm core separation) is 1 meter. This large required separation is due to the weak confinement of the E field parallel to the silicon in a rib waveguide.

3.4 Strip Waveguide

3.4.1 Dimensions

The maximum height and width of a single mode strip waveguide is of the order of tenths of microns which is extremely small and may pose fabrication problems as well as end coupling problems. These small dimensions are due to the large index difference between the silicon core and the air/SiO_2 cladding. In fact, for waveguides which are 0.2 μm thick, the width of the waveguide must not be more than 0.5 μm, in order to ensure that the higher modes are cutoff. The corresponding "cutoff" width for a 0.3 μm thick waveguide is 0.3 μm and that of a 0.1 μm thick waveguide is 0.8 μm. The simulations that I will be running are based on the 3 structures that I have mentioned, i.e. the 0.1 μm x 0.8 μm, 0.2 μm x 0.5 μm, 0.3 μm x 0.3 μm.

3.4.2 Eigenmode Simulations

As opposed to the eigenmode of the rib waveguide, the eigenmode of the strip waveguide extends quite far beyond the silicon core. The reason for this is that, despite the fact that the system is strongly confined, the strip waveguide dimensions have to be extremely small, to ensure that the waveguide has a single eigenmode. This small size results in a significant evanescent field. While the magnitude of the evanescent field is sig-

nificant, the actual horizontal and vertical extent of the evanescent field is on the order of a tenth of a micron. Thus, this means that the waveguide separation has to be on this order for significant coupling to occur, which means that the fabrication of a coupling waveguide would require waveguide separations on the order of a tenth micron. On the other hand, the small extent of the evanescent field also means that cross talk between such waveguides is small for waveguide separation of about a micron and that the density number of such waveguides can be large.

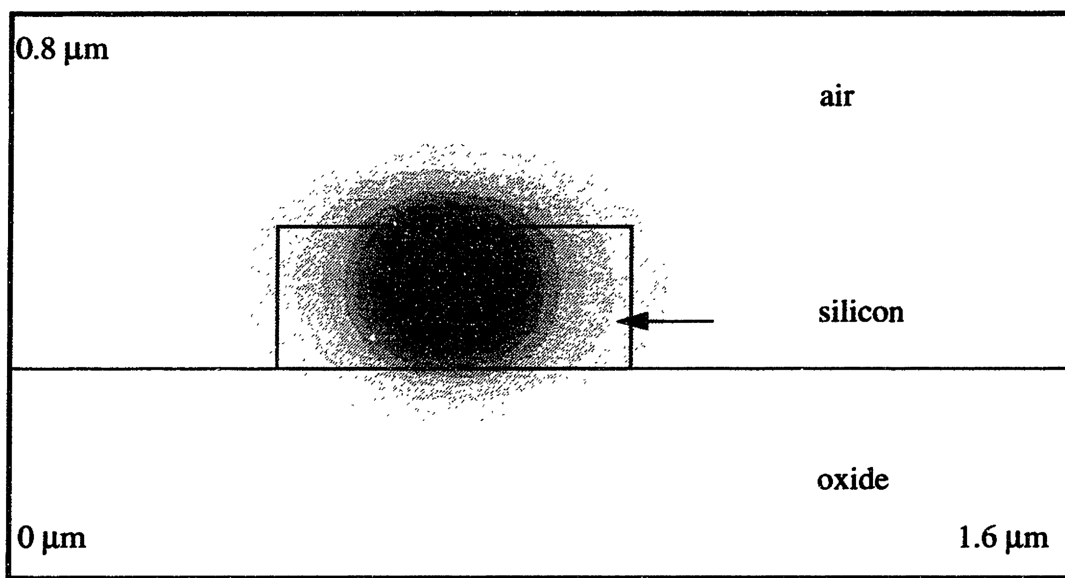

Figure 3.11: Eigenmode of the strip waveguide with dimensions of 0.2 μm x 0.5 μm (Simulation of 80x100 points, scale 40 pts:1 μm)

3.4.3 Loss to Substrate Simulations

As can be seen from figure 3.12, the propagation losses to the substrate are much larger in a strip waveguide than in a rib waveguide for the same oxide thickness. In addition, the losses are related exponentially to the thickness of the substrate oxide thickness. The reason for this exponential dependence of loss on thickness is that the loss mechanism is primarily by coupling of the E field from the waveguide core into the substrate. The E

field "tunnels" through the oxide in an analogous way to tunneling through a potential barrier in quantum mechanics.

Thus in order to get losses on the order of 1 dB/cm, the oxide thickness has to be on the order of 7000Å for both the 0.2 µm x 0.5 µm and the 0.3 µm x 0.3 µm strip waveguide. This large thickness of oxide is beyond the means of SIMOX technology, although other SOI technology such as bonded wafer technology can be used.

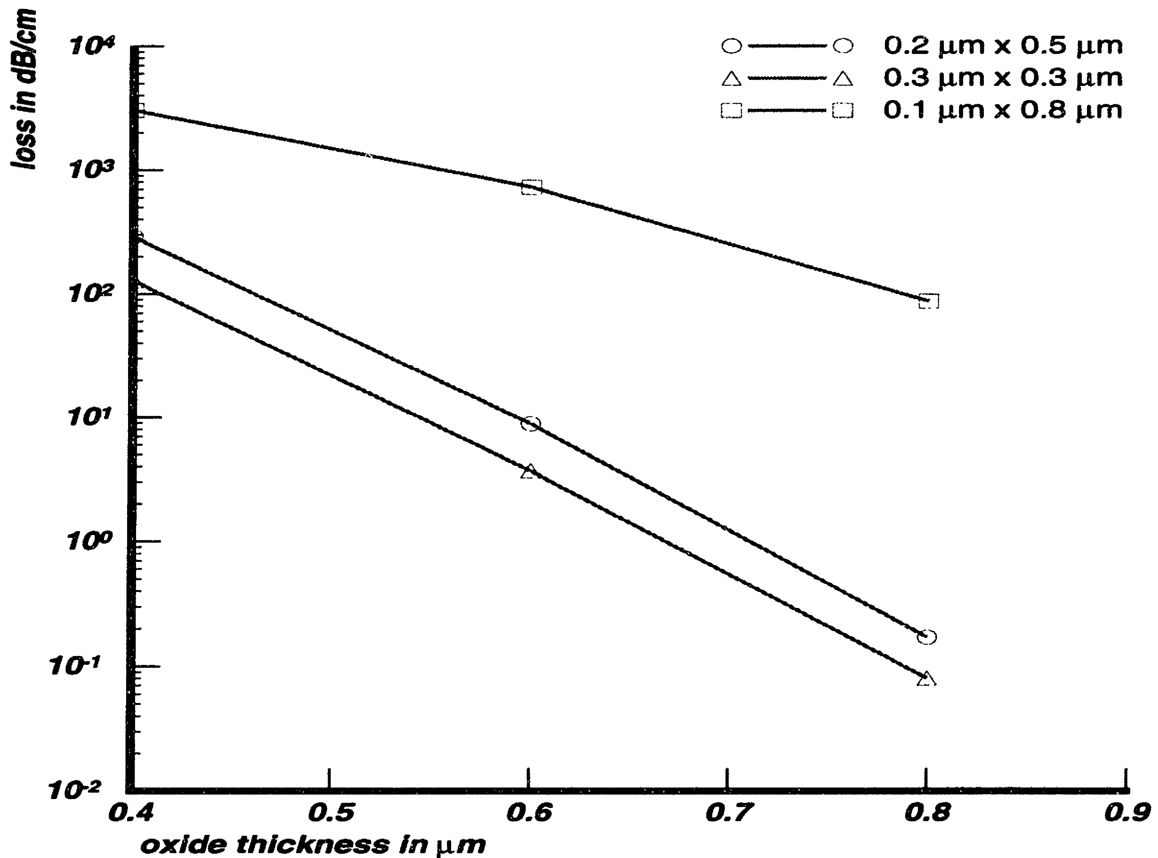

Figure 3.12: Loss in dB/cm vs. oxide thickness in µm for strip waveguides

3.4.4 Bending Loss Simulations

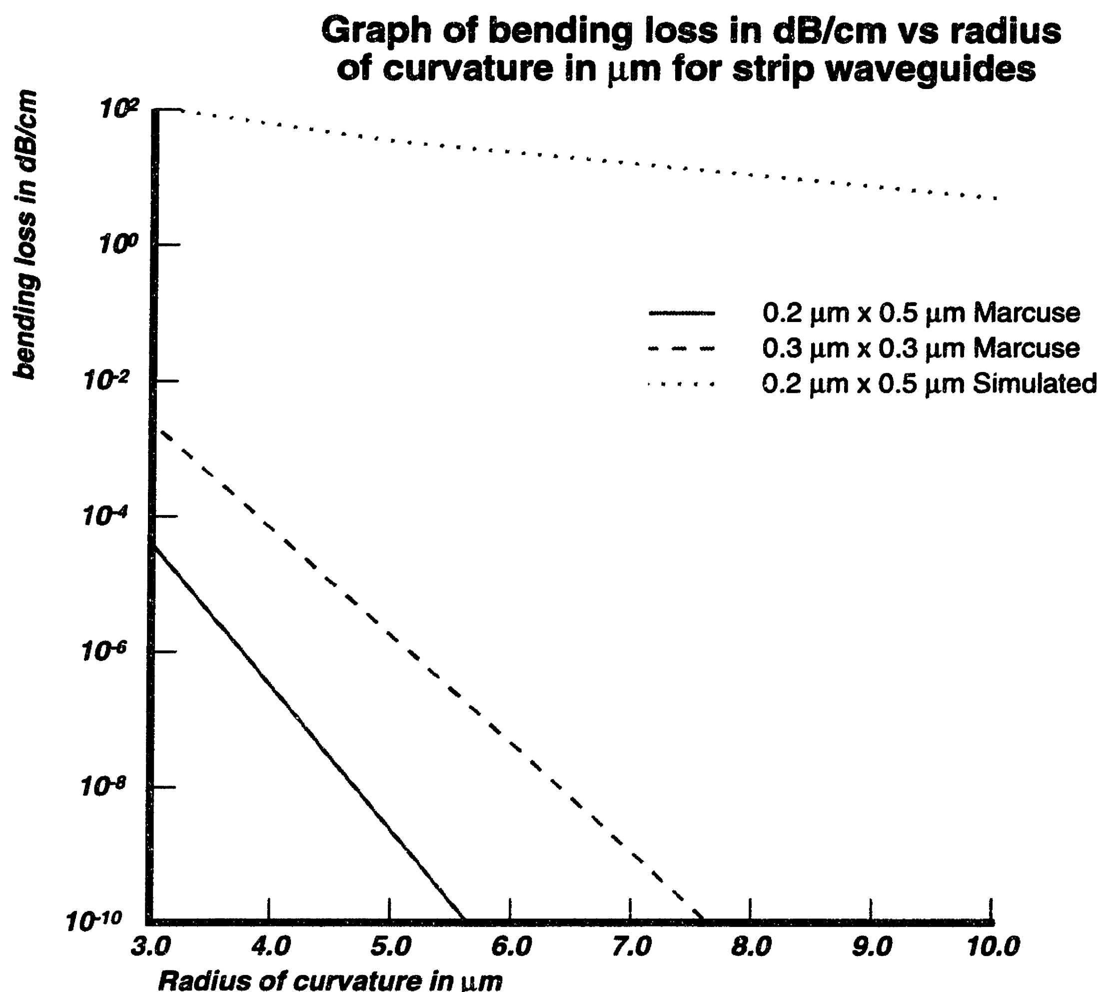

Figure 3.13: Bending loss in dB/cm for strip waveguides of various dimensions vs. bending radius in μm

Bending losses for the strip waveguides were calculated using Marcuse's analysis and by using the beam propagation simulator (see section 2.5.2). As can be seen from figure 3.6, the bending losses associated with the strip waveguide are much smaller as than those of the rib waveguide. For bending radii on the order of microns, the bending losses are on the order of 1dB/cm or less, which is good since this waveguide can be made to undergo sharp bends with low loss. This radius of curvature is about 2 orders of magnitude less than the rib waveguide. In addition, the bending losses associated with the narrower taller

strip waveguide are higher than the corresponding losses of the wider waveguide. This difference is probably not important since the minimum bending radii for losses of 1dB/rad is less than 2 μm for both the waveguides.

Again there are discrepancies between Marcuse's and the simulator. However, this is probably due to Marcuse's slab waveguide approximation, which does not take into account the field confinement normal to the plane of bending. In fact, it is well known that for waveguide with finite width, there is an extra $R^{-0.5}$ dependence of bending loss, which was been neglected in Marcuse's analysis [29]. Also the losses are so small (in terms of losses in dB/90°) that in both cases they are negligible down to 3 μm. This radius is small enough that the assumptions used in the approximations are starting to break down.

3.4.5 Loss to Metal Contacts Simulations

In order to get an estimate for the loss to metallic contacts, the strip waveguides were simulated with a 1 μm Al metal layer deposited on the top surface of the waveguide core. The parameters used for the metal simulation are the same as those used in the simulations for the rib waveguide loss to contacts as described in section 3.3.5. The loss to the metal contact for the 0.2 μm x 0.5 μm, is extremely large, on the order of $6x10^3$ dB/cm, while that of the 0.3 μm x 0.3 μm waveguide is on the order of 3000 dB/cm.

If top contacts are used, one proposal would to use "fingers" for contacts, i.e. alternating p+ and n+ contacts at the top surface of the strips as shown in figure 3.14. In order to achieve losses of less than 1 dB/cm, the metal contacts should cover about 1 in $5x10^3$ of the top surface of the waveguides. The contacts would then be 0.1 μm wide and the separation between the contacts would be 500 μm. It remains to be seen if this contacting scheme is sufficient to cause significant carrier injection, on the order of $10^{18}cm^{-3}$ for index changes of 10^{-3}. Another problem with this contacting scheme is that the current

density through these extremely small contacts could be very large. This may cause high failure rates due to electromigration failure.

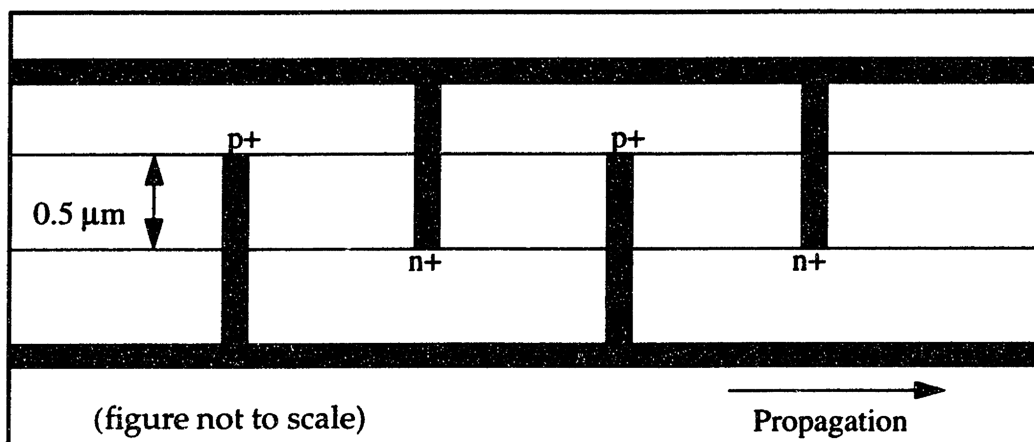

Figure 3.14: Schematic of "Finger" contacting scheme

An alternative method of contacting would be to contact the sides of the strip waveguide. As can be seen from figure 3.11, the lateral extent of the evanescent field of the eigenmode in the 0.2 μm x 0.5 μm strip waveguide is extremely small, so if contacts can be made to the side walls, the losses should be much lower. In fact when a simulation was run with 0.2 μm thick aluminum contacts on each of the side walls, the extracted propagation loss was about 11 dB/cm. This loss more than 2 orders of magnitude less than that of the contact scheme. The formation of side wall contacts without contacting the top is not easy, although the following processing sequence may work:

1. Form silicon on oxide stack.
2. Deposit oxide.
3. Pattern and etch back strip waveguide stack (leave top oxide on).
4. Deposit a conformal layer of polysilicon and perform an anisotropic etch back.
5. Mask and implant p+ and n+ dopants (this requires 2 masking steps).
6. Anneal to out diffuse p+ and n+ dopants from silicide/polysilicon.
7. Strip polysilicon and contact to the silicide.

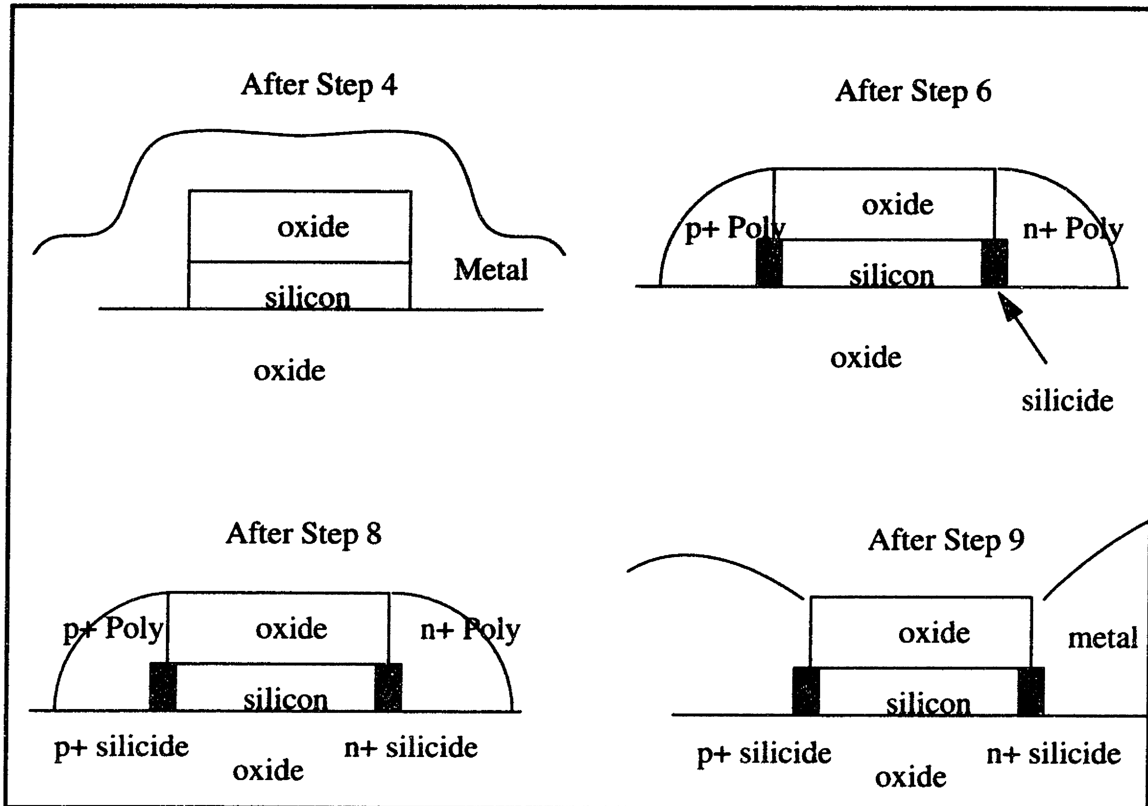

Figure 3.15: Schematic of contacting

The reason why polysilicon is proposed as a means of contacting the sides of the strip waveguide is that very shallow junctions are required in this technology to minimize absorption losses near the contact. A 1000Å wide profile should probably suffice, although this dimension is much smaller than standard lithography techniques will allow. The polysilicon acts as a diffusion source of dopants from which a shallow p+ junction may be formed.

The two contacting schemes may be combined to provide low loss, metal contacts which may the means to inject carriers into the strip waveguide, i.e. the combination of "finger contacts" with side wall contacts.

3.4.6 Ease of Fabrication

To get losses to the substrate on the order of 1 dB/cm, the oxide thickness below the strip waveguide core has to be approximately 7000Å, which is not possible with SIMOX technology. Thus, bonded wafer technology has to be used in order to fabricate these structures, if the waveguide core material is to be single crystal. In order to solve this problem, Koker has proposed polysilicon on oxide waveguides [10]. The advantage of these waveguides is that single crystal SOI technology is not required, since the polysilicon can be deposited on the oxide, a process frequently used in CMOS technology.

Although the 0.3 μm x 0.3 μm waveguide is at the limit of UV lithography technology and poses significant constraints on field alignment, the dimensions which have been mentioned should be routinely achievable in manufacturing lines as 0.35 micron and 0.25 micron CMOS technologies mature. The 0.1 μm x 0.8 μm waveguide is probably non-optimal since its losses to the substrate are large, while the 0.2 μm x 0.5 μm waveguide shows higher losses to substrate than the 0.3 μm x 0.3 μm waveguide, although the bending loss for the second waveguide is smaller than the last. In addition, the losses to metal in the side contacting scheme will be smaller for the wider waveguides. The reverse will be true for the top contact waveguides, that is, the losses to contacts will be smaller for the narrower but taller waveguides.

The strip waveguide affords significant advantages as it exhibits smaller bending losses and smaller geometries than the larger rib waveguides which makes it ideal for interconnects. However, these advantages may not be realized in the near future since the coupling losses light from the light sources to the strip waveguide will be much larger the rib waveguide since the cross sectional area of the strip is so small.

On the other hand., the radiation losses of strip waveguides to the substrate is large. In addition, the strip waveguide exhibits high scattering losses at the silicon/air interface.

The surface roughness as a result of an anisotropic dry etch which is required to etch the vertical side walls of the strip waveguide will exacerbate the scattering losses of the strip as well as the rib waveguides. A possible fix to this problem would be to form the vertical sidewalls with an anisotropic dry etch and to smoothen the wall using an isotropic wet etch [27]. Alternatively an anisotropic wet etch can be used to etch the side walls. The etch step should be followed by a thermal oxide step, which would serve both to electrically passivate the sidewalls as well as to reduce the rms roughness of the walls, which would in turn reduce scattering losses.

Chapter 4

Modulator Design

4.1 Rib Waveguide Coupling Modulator

4.1.1 Dimensions of Simulated Structure

Modulators based on the rib waveguides were simulated using beam propagation, process and electrical simulators. The beam propagation simulations show the feasibility of the device from the "optical" point of view and will give the estimated values for the loss, the required length, the modulation depth and the electric field distributions of the modulator. Device simulations were performed on the AT & T simulator, PADRE to examine the feasibility of injecting large amounts of carriers. The process simulations were run on the process simulator PROPHET to give realistic inputs to PADRE. The simulated devices had dimensions of 5 μm by 3 μm, with a waveguide core separation of 6.8 μm (a 0.8 μm gap) and a core separation of 7 μm (1 μm gap). The coupler with the 6.8 μm separation had a coupling length of about 600 μm, while the coupler with the 7 μm separation had a coupling length of about 900 μm. The results of preliminary simulations can be seen in figure 4.2, figure 4.4 and figure 4.5. This device is by no means optimized but is meant to demonstrate the feasibility of the electro-opto modulator.

4.1.2 Eigenmode Simulations of Rib Coupler

The first eigenmode of the rib coupler with dimensions of 5 μm by 3 μm and a waveguide separation of 7 μm is shown in figure 4.1. This plot is consistent with the schematic shown in figure 2.3. The first eigenmode, which has lower energy, is symmetric and it can be shown that the second eigenmode is anti-symmetric. The symmetry of the first mode implies that the field is non-zero between the waveguides. This is unusual since in

most coupling devices, the electric field of the first eigenmode is antisymmetric. The reason for the antisymmetry in most coupling devices, is that the index of refraction between the waveguides is much lower than the index of the core. Thus, the propagation constant for the antisymmetric first mode is larger than that of the symmetric second mode which has non-zero E field in the low index region between the cores. However, in the case of the rib waveguide coupler, the E field can stay in the high index silicon bridging between the cores. In fact, in this case, the symmetric eigenmode has a lower propagation constant than the antisymmetric one, since in the antisymmetric case, a larger portion of the E field resides outside the silicon core.

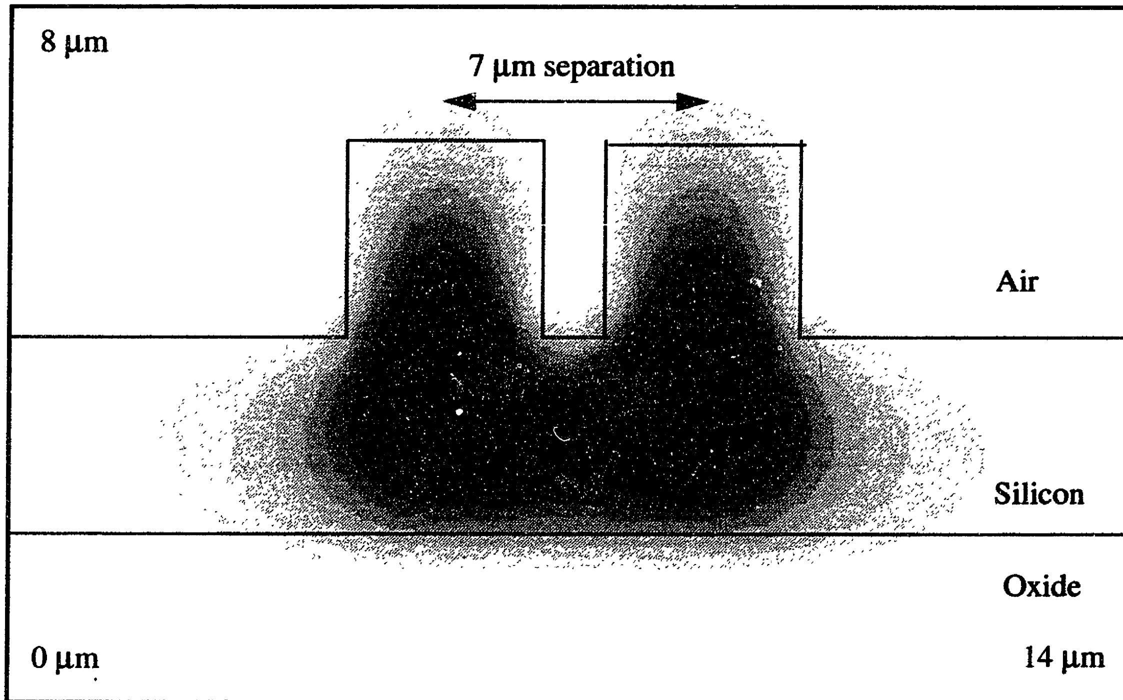

Figure 4.1: First eigenmode of rib waveguide coupler with width = 3 µm and height = 5 µm (Simulation of 140x80 points, scale 10pts:1 µm)

When the eigenmode E field of each of the waveguides taken singly is launched in one of the two waveguides, the two lowest modes will be excited. These two modes then propagate down the waveguide at different velocities, giving rise to power switching back and

forth from one waveguide to the other. Changing the index in guide I, changes the eigenmode profile of the system, as was described in section 2.4. This changes both the coupling length and the maximum power transfer between the two waveguides.

Another important feature of the eigenmode simulation is the fact that the E field is confined to the silicon in the core and cladding. This should come as no surprise, since the index of refraction of silicon is much higher than that of the air or the oxide. In fact, the eigenmode simulations of the rib waveguide showed similar characteristics (see section 3.3.2). Furthermore, the eigenmode of the coupling waveguide should be, to a close approximation, the sum of the first eigenmode of each waveguide taken in turn. Thus most of the discussions about loss for the rib waveguide in the previous chapter can be generalized to the rib waveguide coupler.

4.1.3 Simulation of Coupling in Rib Waveguides

The results presented here are for the rib waveguide with dimensions of 5μm by 3 μm and a waveguide separation of 6.8 μm. An index change of 3×10^{-3} was used in the simulating, as this was the minimum index of refraction that gave almost full modulation at the output.

The trench between the waveguides was simulated with index of 1.48, which is equivalent to SiO_2 filling the trench. This value does not significantly change the eigenmodes in relation to an air trench, since the index difference in both the Si/air system and the Si/ SiO_2 system is large. Furthermore, this is a more realistic simulation, since a passivating thermal oxide layer is needed both to smoothen the side walls. As was mentioned in the previous chapter, this thermal oxide will reduce scattering losses and will electrically passivate the etched back silicon, which will in turn reduce leakage currents along the sidewalls.

The simulations were run with the assumption that the initial beam was incident on the right waveguide and that the incident E field profile is the eigenmode one of the 2 waveguides taken singly.

The results of the simulations are shown in figures 4.2-4.5. Similar profiles can be obtained for any single mode rib waveguide system with a reasonable waveguide separation. Figure 4.2 is a plan view of the waveguide coupler in which the E field is set off in the bottom waveguide labelled Waveguide I. The figure shows the intensity of the E field coupling from Waveguide I (on bottom) to Waveguide II (on Top). The simulation was run with 140 x 300 points, representing a simulation domain of 14 μm vs. 600 μm. The dark areas indicate regions of high peak field intensity.

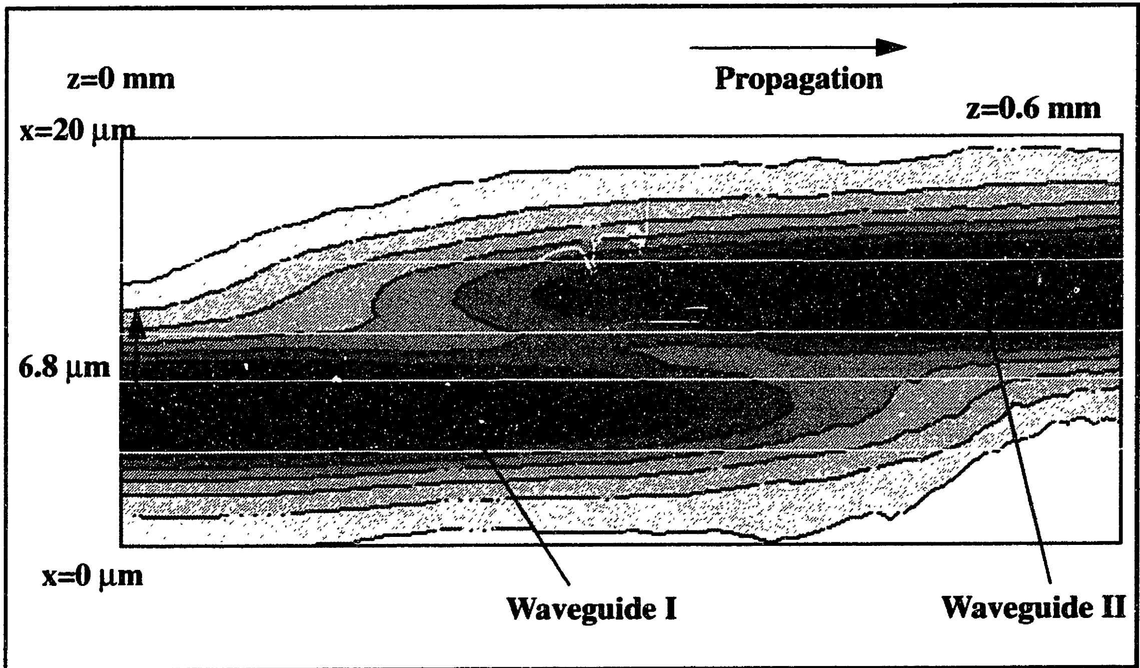

Figure 4.2: Plot showing coupling of E field in rib waveguide (Δn=0)

As can be seen from the plot, when the difference in index, Δn, between guide I and guide II is zero, the coupling length of the modulator with 6.8 μm core separation is 600 μm. On the other hand when the index of refraction of waveguide II is reduced by Δn=-

$3x10^{-3}$, the power transfer from waveguide I to waveguide II is negligible and the power remains largely in waveguide I as shown in figure 4.2.

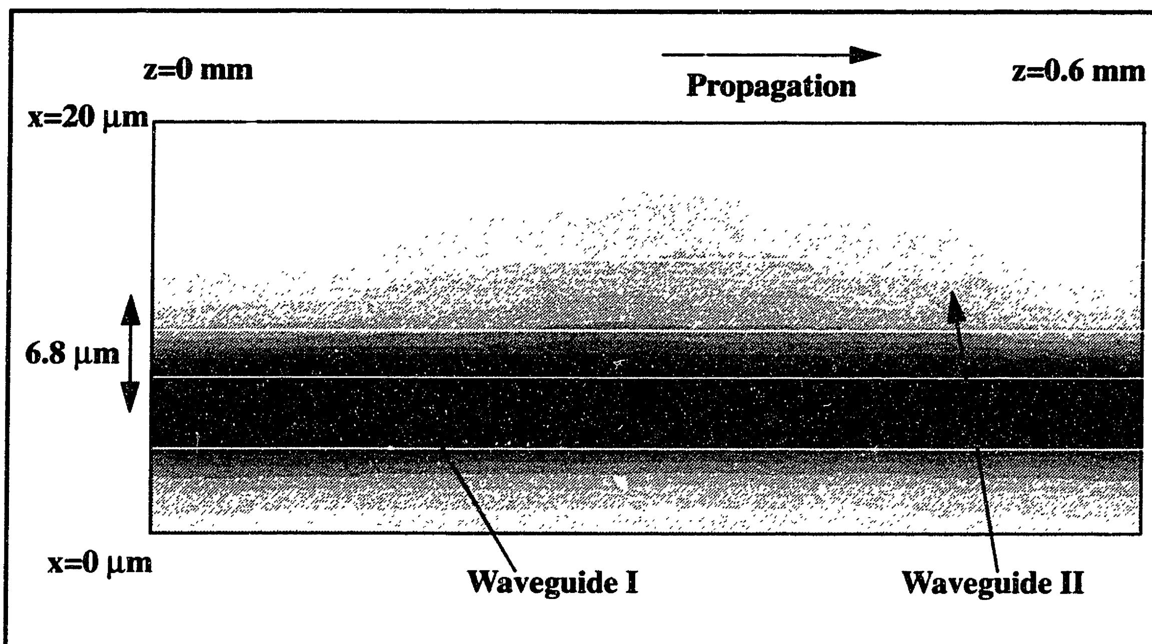

Figure 4.3: Plot showing coupling of E field in rib waveguide ($\Delta n=-3x10^{-3}$)

Figures 4.4 and 4.5 show the cross sectional E field intensity of the rib waveguides. The simulation was run with 140 x 80 points, representing a simulation domain of 14 μm vs. 8 μm. Again the dark areas indicate regions of high peak field intensity, with the incident E field set off in the right waveguide, labelled waveguide I.

Figure 4.4 shows that there is full power transfer from guide I to guide II in 600μm as was the case with figure 4.2. However, when free carriers are injected into waveguide II, the magnitude of power transfer decreases greatly as shown in figure 4.5 and most of the power remains in waveguide I. In addition, the coupling length decreases from a value of 600 microns to approximately 300 microns when the index of waveguide II is reduced by $3x10^{-3}$.

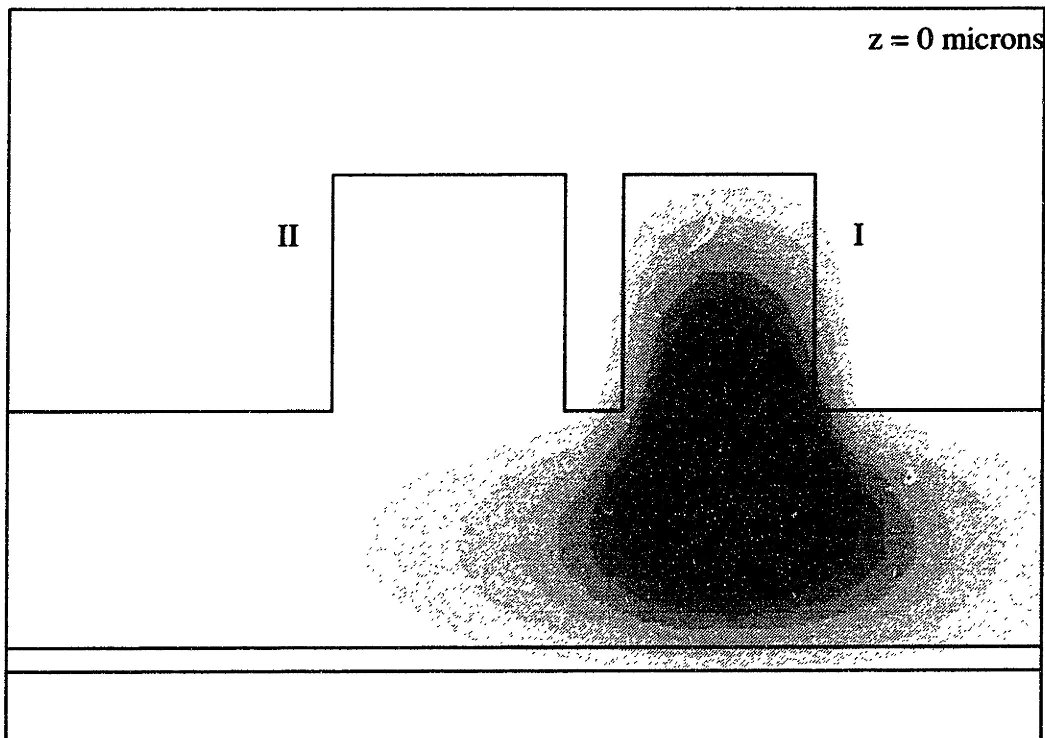

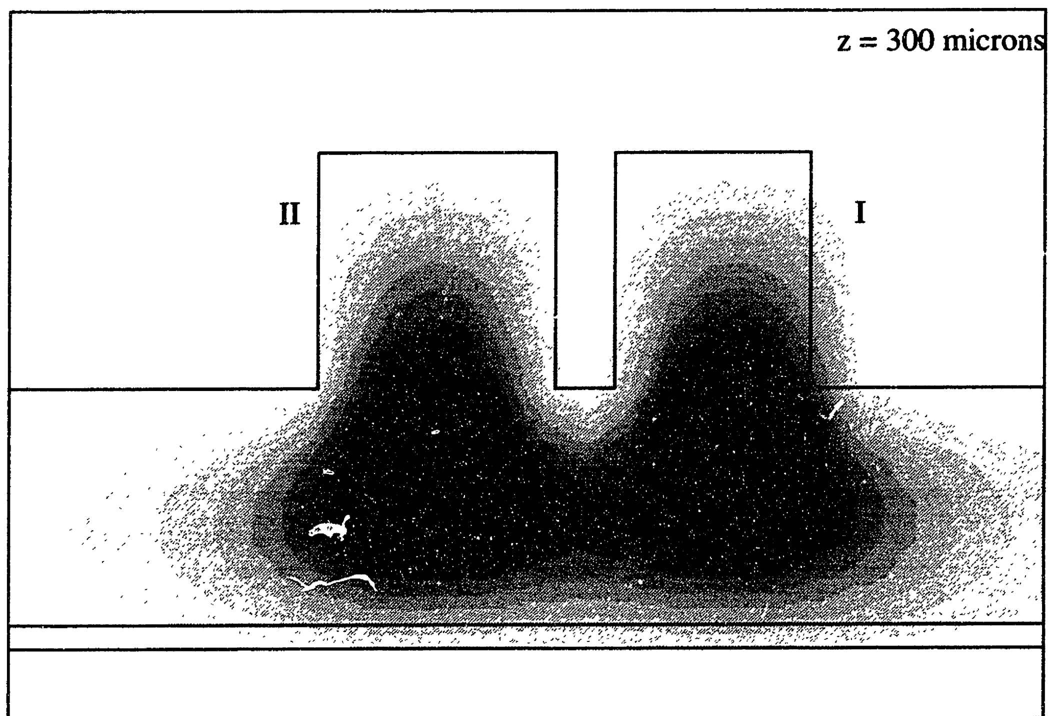

Figure 4.4: Graph showing the evolution of E field with $\Delta n=0$

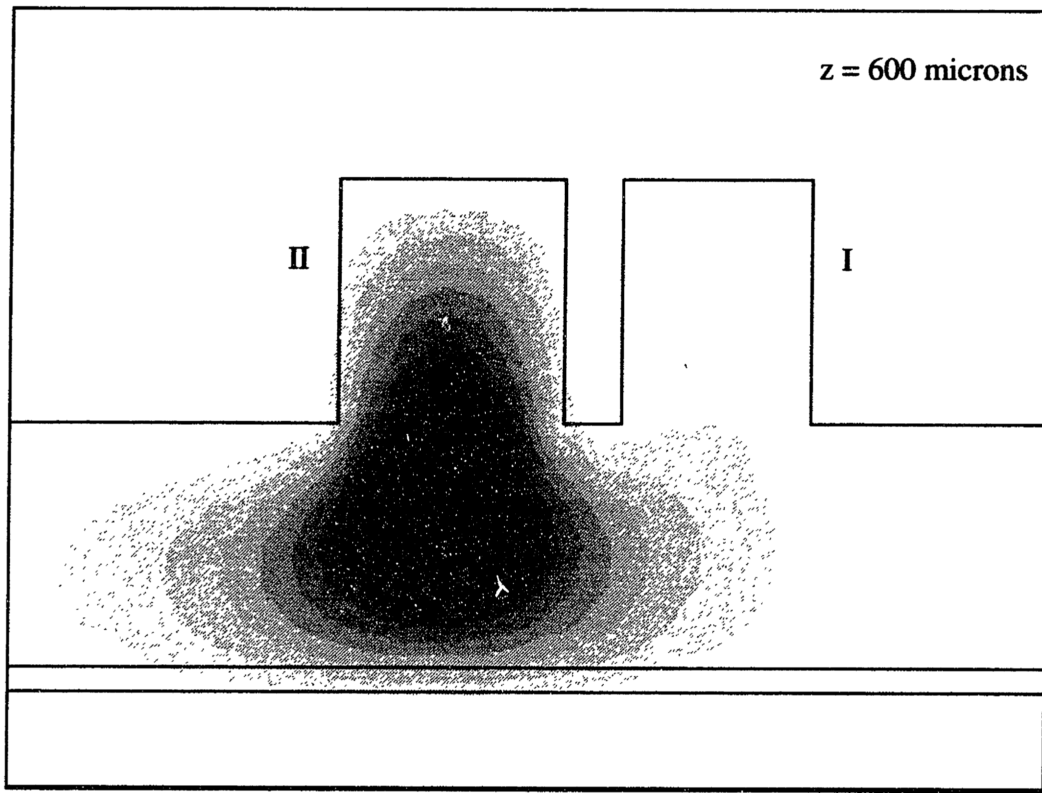

Figure 4.4 cont'd: Graph showing the evolution of E field with $\Delta n=0$.

Although the power transfer from waveguide I to waveguide II is a maximum at 300 microns, the magnitude of the peak power transfer is much smaller than when the index difference is 0. The reason for this large change in power transfer, despite the small index change of $3x10^{-3}$, can be understood by comparing the effective indices of the core and the cladding, which are 3.477 and 3.467 respectively. The difference in effective index between the core and the cladding is only $\Delta n=10^{-2}$, compared with a simulated free carrier refraction change of $3x10^{-3}$. Thus small index changes can bring about large changes in the mode profiles, which in tuns greatly affects the maximum power transferred between the waveguides. See section 2.4. This makes the coupling modulator extremely attractive since the free carrier refraction is not very large.

As the index of refraction of waveguide II is varied, the coupling length of the modulator as well as the maximum power transferred changes. Since the power transfer between the waveguides is so large with a small index change, the magnitude power transfer is relatively insensitive to changes in the index of refraction of guide II.

This design is also attractive because the carrier injection levels and hence the applied voltages do not have to be within tight tolerances, unlike phase modulators or other coupling modulators, which are based on coupling length changes. The operating point of this device can be chosen such that the power transfer is low since the effect coupling length is relatively unimportant. Thus, as long as the first structure is built to approximately to specifications and is symmetric, almost full power transfer should occur between the waveguides. The main effect of a varying level injection or device length would be a small change in the modulation depth, or the efficiency of the modulator.

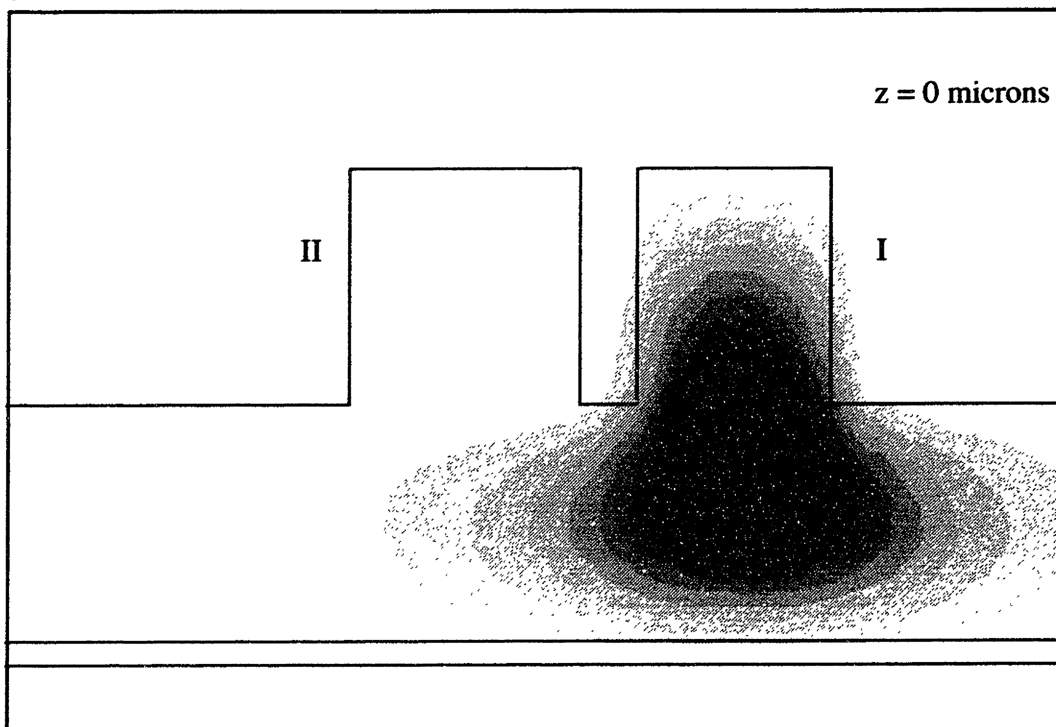

Figure 4.5: Graph showing the evolution of E field with $\Delta n=-3x10^{-3}$.

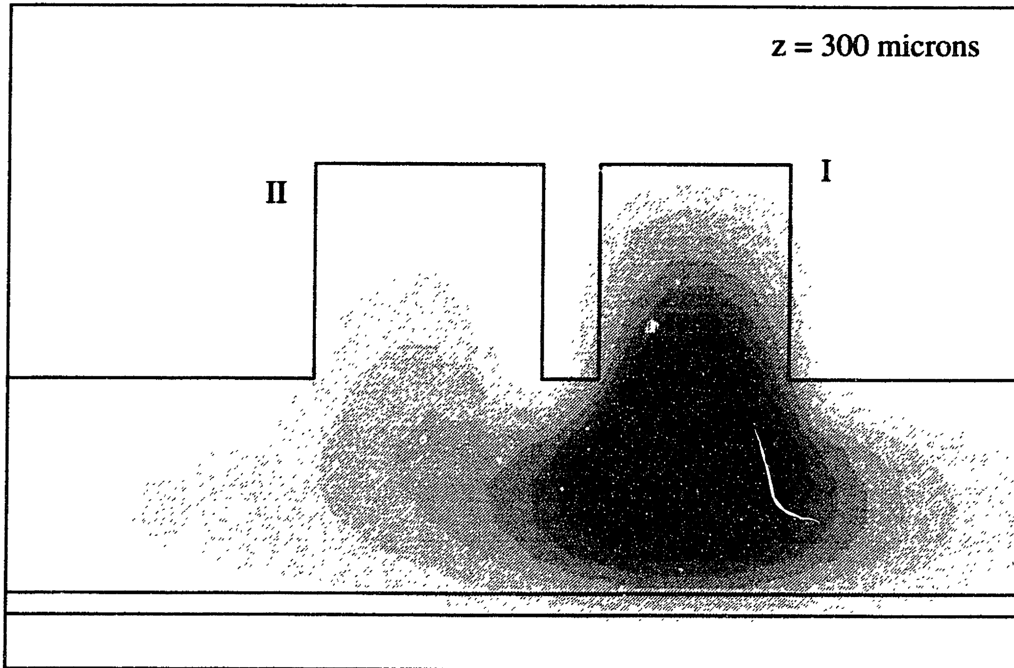

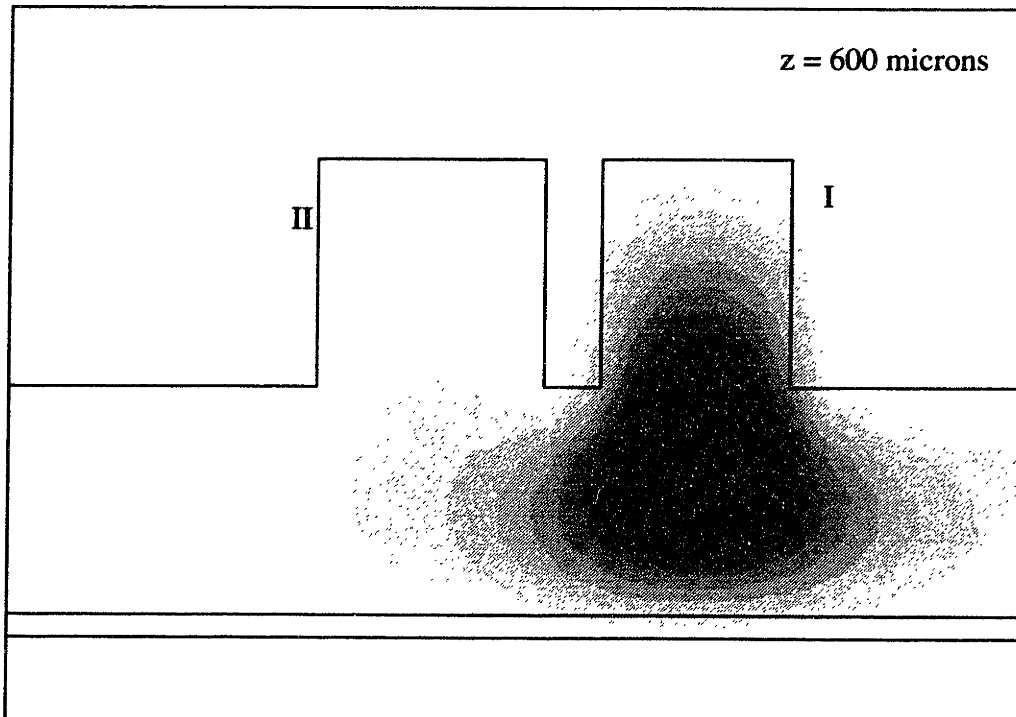

Figure 4.5 cont'd: Graph showing the evolution of E field with $\Delta n=3x10^{-3}$

The length of the modulator is an important dimension of the device. If the modulator is made too long, it will take up too much space and will require high power to drive. On the other hand, in order to reduce the length of the modulator, the coupling length must be reduced, most effectively by reducing the separation between the guides. The trade off is a reduced separation between the waveguides against an increased sensitivity to process variations on the critical dimension, the waveguide separation.

The modulation depth

$$10 \times \log \left(\frac{I_{max} - I_{min}}{I_{min}} \right) \tag{4.1}$$

is about 20 dB for the 3 μm by 5 μm modulator with 6.8 μm separation.

4.1.4 Loss Simulations of the Rib Waveguide Coupler

In order to understand the losses associated with propagation down a waveguide, the waveguide coupler was simulated with a 2000 Å thick oxide layer, which would make it compatible with SIMOX technology. This finite oxide thickness will result in some loss due to coupling to the substrate as was mentioned in section 3.3.3.

To model the losses associated with the metallic contacts to the silicon, simulations were run with 1μm of aluminum deposited at the top of the waveguides. These contacts are necessary for the operation of the p-i-n diodes, as they will be used for the injection of free carriers which will in turn cause free carrier refraction.

In addition to the metal absorption coefficient, a free carrier absorption coefficient of 11 cm^{-1} was used in waveguide II, to simulate the total loss due to the free carrier absorption effect during carrier injection. This absorption coefficient corresponds to a hole injection of 10^{19} cm^{-3}, and gives an index change of -10^{-2} which is larger than the value with which this device was designed. Despite this large amount of carrier injection, the extracted propagation loss is low.

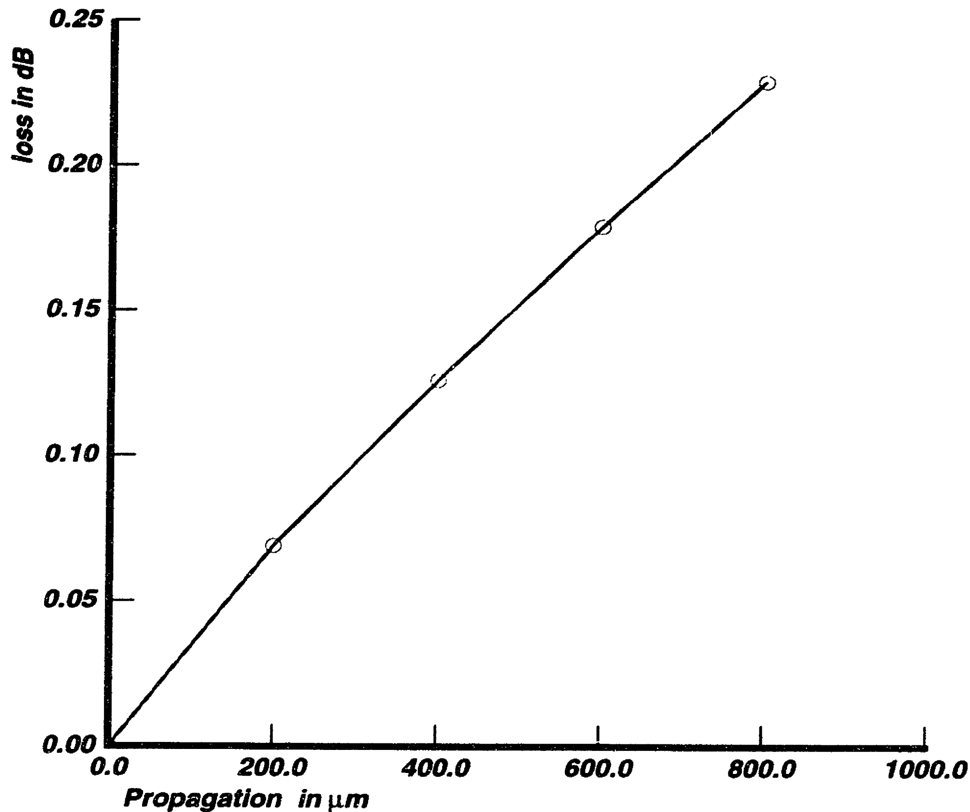

Figure 4.6: Plot of loss in dB to substrate, carrier injection and metal vs. propagation distance.

Note, however, that scattering losses which will account for a significant amount of propagation losses have been neglected in these simulations. See section 3.2.2.

The loss to the substrate and metal can be extracted from figure 4.6, which is a plot of loss in dB to the substrate, injected holes and metal contacts vs. propagation distance. The total loss is less than 0.5 dB (5% loss) for the entire length of the modulator, so the problem of loss to the metal contacts is reasonably small as is expected for the simulations with the rib waveguides.

One advantage of this design is that the peak concentration of the injected carriers is outside the peak E field of the mode. This design enables modulation to occur without sig-

nificant losses to the free carrier plasma effect mentioned in section 2.2. This low loss is despite the fact that the required injection level is high -- in order to attain a change of index $\Delta n=-3x10^{-3}$, the injection level must be at least $2x10^{18}cm^{-3}$.

With this magnitude of index change, a modulator based on phase modulation and interference, e.g. the Mach Zehnder modulator, is about 200 μm long. This length is a factor 3 shorter than that of the coupling modulator which I have simulated. However, the theoretical absorption losses associated with such a phase modulator will be about 4 dB (60% loss). Furthermore, Mach Zehnder based modulators require bends, which have result in significant losses for rib waveguides.

4.1.5 Process Flow and Process Simulations

The optical simulations indicate that the rib waveguide modulator is possible, if a change in the index of refraction of $\Delta n = 3x10^{-3}$ is assumed. This corresponds to a hole injection of $2x10^{18}cm^{-3}$. In order to ensure that this level of injection is possible, electrical simulations were run. Process simulations were run on PROPHET to give "real" dopant distributions as inputs to the PADRE electrical simulator.

Since a process simulator like PROPHET simulates a sequence of steps, such as diffusion and implantation, it is necessary to design a process flow which could be used to fabricate the modulator. A possible process flow is shown in figure 4.7.

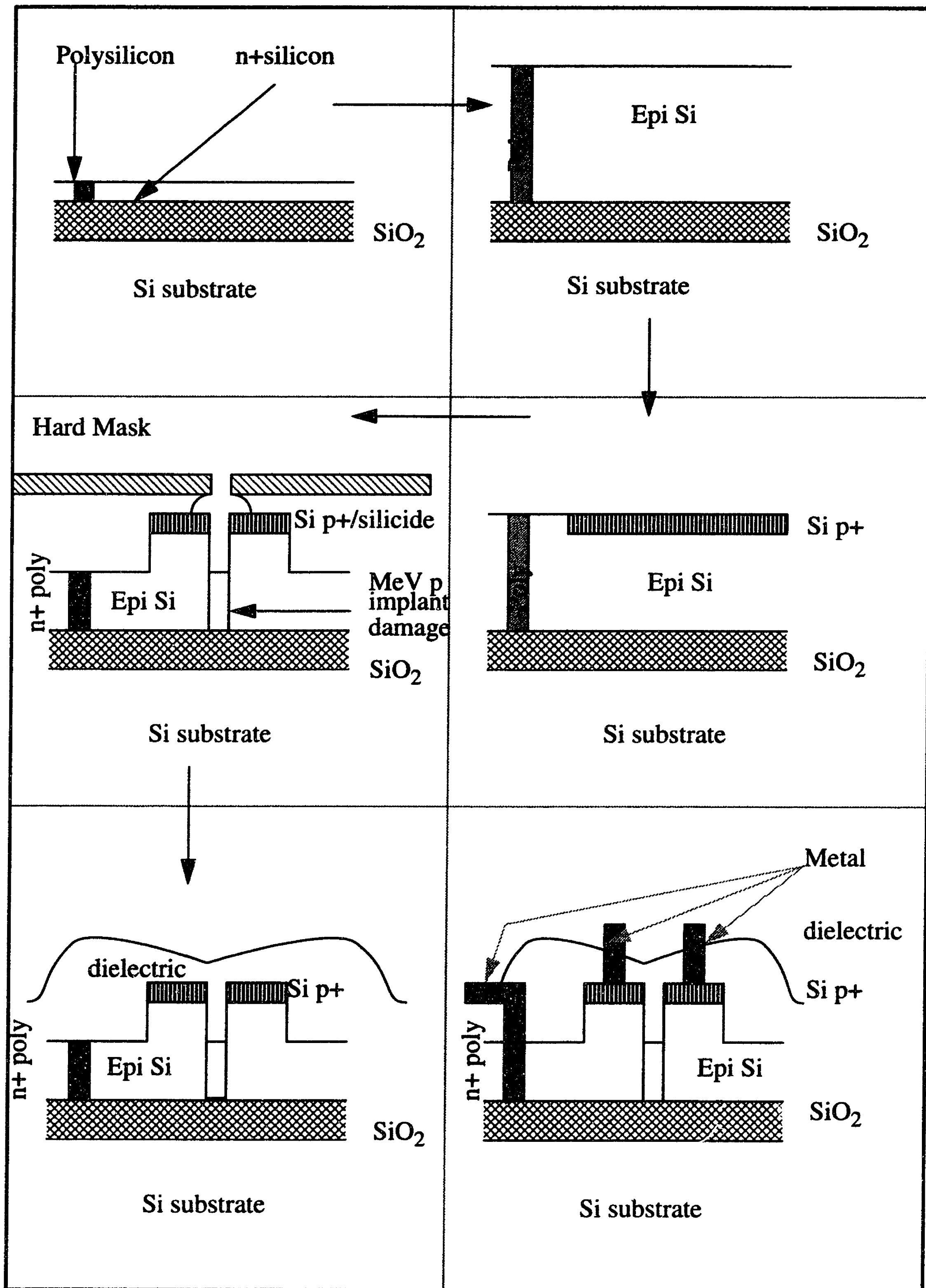

Figure 4.7: Schematic of process flow for rib waveguide modulator (not drawn to scale)

The process steps may be summarized as follows:

1. Implant oxygen and anneal for SIMOX formation,
2. Pattern and etch back Si for polysilicon formation,
3. Non selectively deposit LPCVD lightly doped silicon & 0.1 μm p+ silicon to a total silicon thickness of 5 μm,
4. Implant BF_2^+ at 10keV and a dose of $5x10^{15}cm^{-2}$,
5. Deposit Metal I stack for silicide formation, e.g. Co or Ti,
6. Pattern and partially etch back rib pattern using RIE and metal as hard mask,
7. Pattern and implant contact to buried layer (High energy/high dose P implant),
8. Anneal to form silicide and to activate the boron and phosphorus dopants,
9. Wet clean and etch + thermal oxidation to smoothen sidewall,
10. Deposit PECVD oxide with good step coverage,
11. Deposit hard mask to protect shelves from proton bombardment,
12. Pattern hard mask and wet etch oxide from the trench,
13. Deposit LTO or PECVD oxide for trench filling and planarization,
14. Implant P at low energy to passivate the etched trench followed by an anneal,
15. [1]Implant MeV protons at high dose,
16. Pattern contact holes and etch to open contact holes and
17. Deposit Metal II and sinter to contact.

The starting material should be a silicon on oxide SIMOX structure with an oxide thickness of 0.2 μm which is consistent with the optical simulations. The reason for step 2, the etch back of the silicon followed by the regrowth of polysilicon is to create a deep electrical contact to the silicon. Since the diffusion of dopants in polysilicon due to grain boundary diffusion is rapid, an ohmic contact can be formed with ease using the polysilicon. The purpose of this large contact is to create a large sink for injected carriers by auger

---

1. The temperature of all subsequent steps should not exceed 200°C which put severe constraints on subsequent back end processing steps [43].

recombination. In addition, the large area of the contact makes carrier injection more efficient. The importance of these two effects will become apparent in the next section.

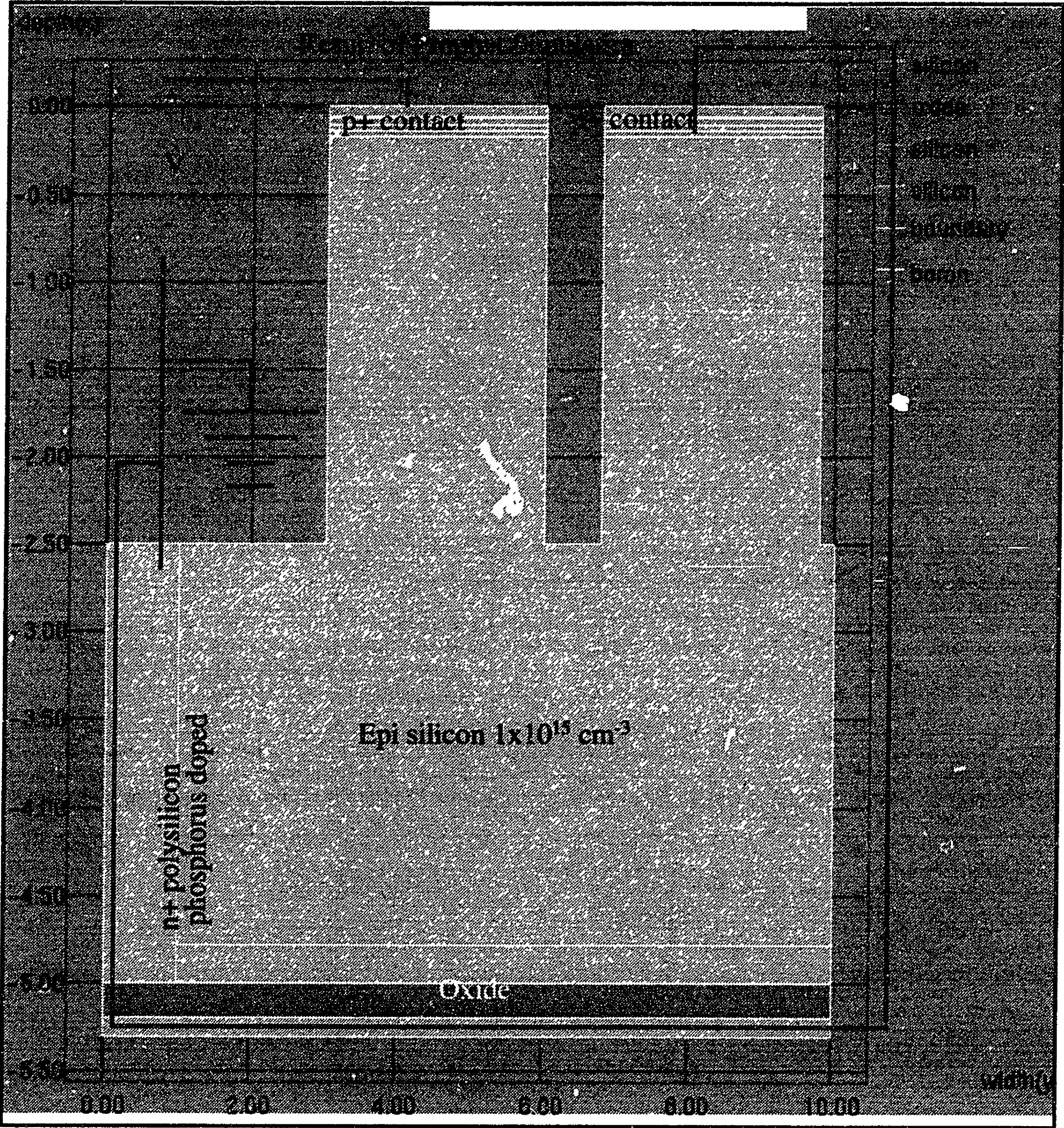

Figure 4.8: Result of the 2 D Prophet simulation

The CVD grown material was simulated with a concentration of 10^{15} cm^{-3} because it is difficult to deposit intrinsic silicon using CVD methods. The reason for this is that the

background doping concentration of reactor will result in a finite and significant amount of dopant being deposited with the silicon. This level of doping is not a problem since the absorption losses due to 10^{15} cm^{-3} doped single crystalline silicon is negligible as was discussed in section 2.2.

Most of the processing after the CVD silicon step is involved in the patterning and etching the rib waveguide structure. Another important process step, as will become apparent in the next section, is the MeV proton bombardment which may be required for damage creation in the region of the coupler adjoining the two cores. The need to maintain the proton damage puts a severe constraint on the back-end processing, since the temperature of any subsequent step must be less than 250 °C. Fortunately, Plasma Enhanced Chemical Vapor Deposited (PECVD) oxides can be deposited at this low temperature.

The entire process was designed on the premise that shallow heavily doped contacts result in high levels of injection per unit voltage applied to the contacts, as is the case in the paper by Tang et al. [11]. Thus, careful consideration was made to minimize the thermal budget of the processes. As a result after SIMOX formation and the CVD growth steps, the process flow has a small total thermal budget. This implies that standard IC processing may be carried out after the CVD growth step for fabrication of the electronics circuits and driver circuits for optoelectronics applications.

In addition, low energy, high dose BF_2^+ implants which are routinely used in shallow source/drain formation, were used to form the p+ contact. The dose of boron implant used for the top p+ contact was $5x10^{15}cm^{-2}$ at an energy of 10keV and the thickness of the doped p+ layer was less than 1000 Å. This had the further advantage of minimizing the losses due to the free carrier plasma effect. The n+ contact, formed by the degenerately doped polysilicon, was made on the partially etched shelf, approximately 2 μm away from the core edge to minimize losses.

In order to save simulation time, I assumed a uniform doping of 10^{20} cm^{-3} for the polysilicon and performed only a single 1000 °C anneal to model the thermal budget of the oxidation process. The result of the process simulation is shown figure 4.8.

4.1.6 Electrical Simulations

As has been mentioned previously, electrical simulations were performed on the AT &T simulator PADRE. Both 1D and 2D simulations were calculated for rib waveguide structures to study the electrical characteristics of the device. 1D simulations are important in determining if $10^{18}cm^{-3}$ injection levels are possible with p-i-n diodes fabricated in the waveguides, while 2D simulations are important in examining 2D effects such as current crowding and electrical isolation of one waveguide from the other.

The simulations once again assumed a waveguide with a height of 5 μm and width of 3 μm together with a core separation of 6.8 μm. I will only present the results of the 2D simulations because the 1D results are encompassed in the 2D results.

The results of the 2D PADRE electrical simulations are shown in figure 4.9 and figure 4.10. In these simulations, a positive voltage was applied to the p+ contact at the top of the rib waveguide II, while the other p+ contact on waveguide I and the n+ contact was grounded. In effect, a p-i-n diode of length of about 5 microns was simulated. The plot showing the hole concentration at V = 0V shows the approximate doping concentration which was set up by using PROPHET simulations.

As is apparent from the simulations, it is relatively easy to achieve high levels of injection of $2x10^{18}cm^{-3}$, with a relatively small voltage of +1.2 volts applied to the top contact with respect to the grounded n+ contact. These injection levels increase with increasing voltage. In fact, 10^{19} cm^{-3} injection levels are possible with applied voltages as low as 2 volts. However, as will become apparent later, these devices require large amounts of cur-

rent drive and hence the power dissipated by these devices are large. Thus I have chosen to keep the operating voltage to as low a level as is possible. It is necessary to control the Ohmic heating of the device, since a rise in temperature causes an increase in the index of refraction, which may counteract the reduction in the index by the free carrier refraction effect. This effect was neglected in the simulations presented here.

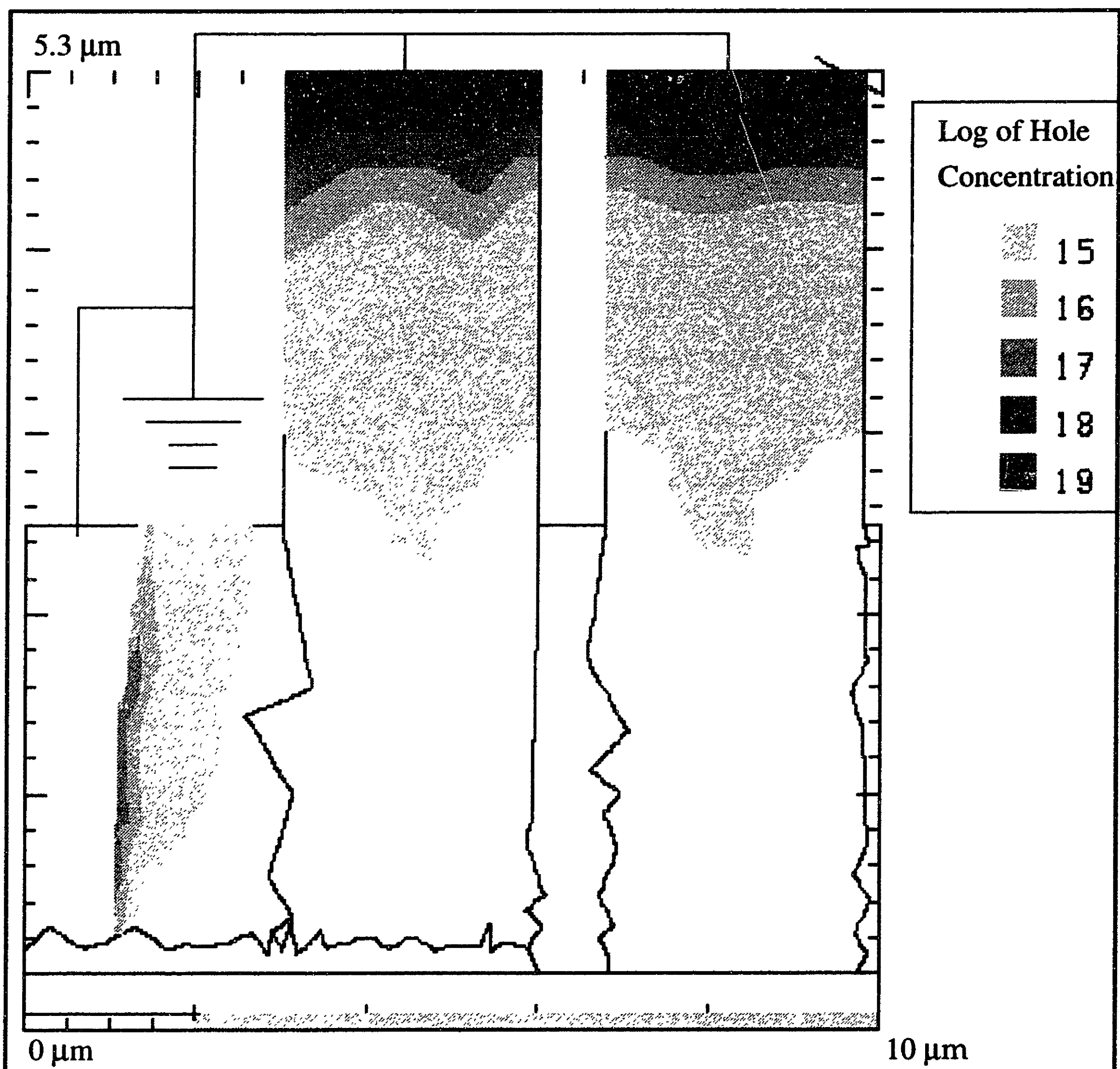

Figure 4.9: Padre simulation of hole concentration at an applied voltage of V=0V

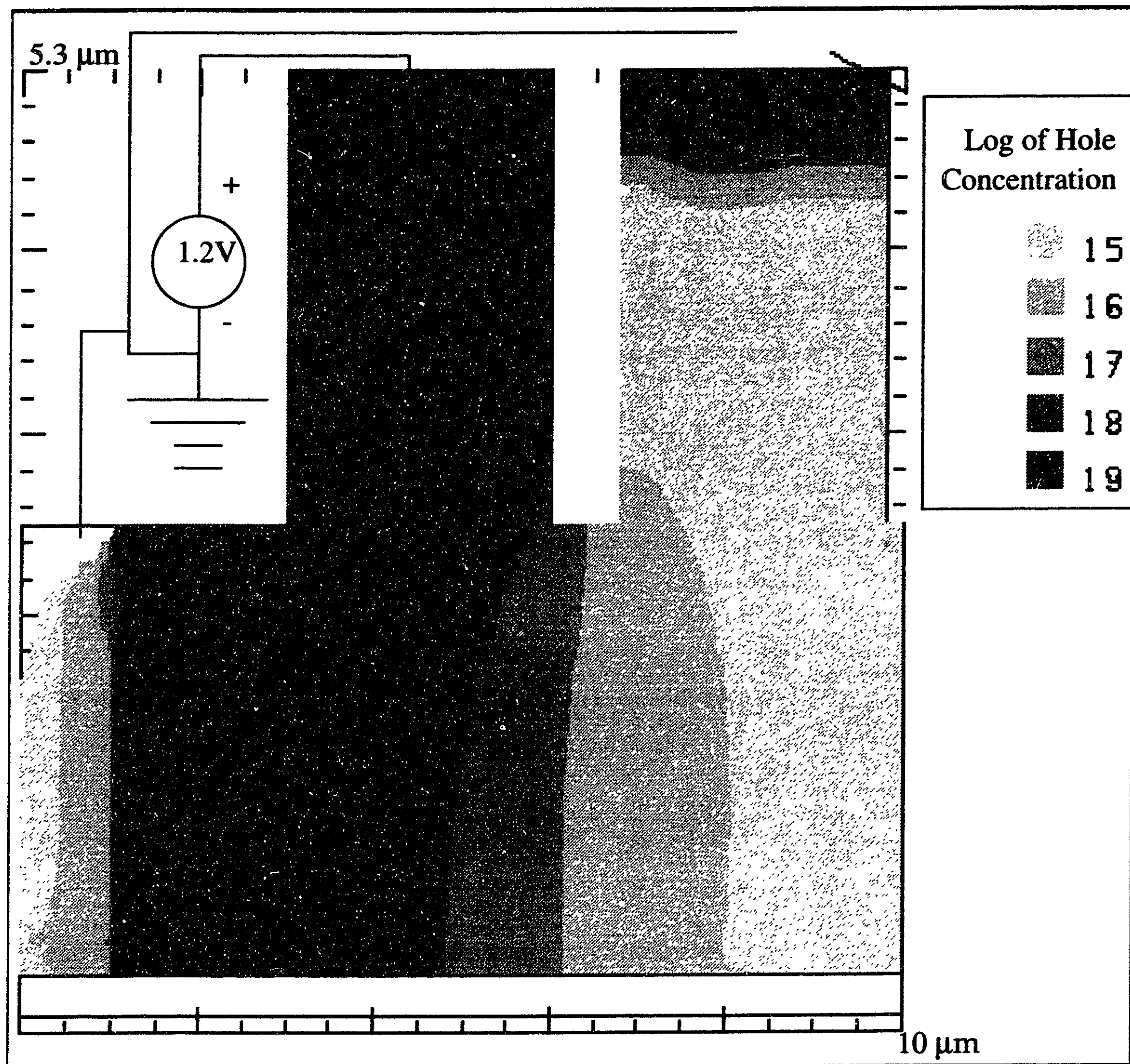

Figure 4.10: Padre simulation of hole injection concentration when the p-i-n device is in the on state or voltage drop between the p+ and n+ contacts is 1.2V

Although high level injection of electron and hole concentrations are easily achievable, the isolation of carriers from one waveguide to the other is still a hard problem to solve. The reason is that the carrier diffusion length is large enough in lightly doped material that the carriers will diffuse into the other waveguide. This is an important problem to consider, because if the free carriers are not properly confined to one of the waveguides, then the modulator loses performance. The reason for this loss in efficiency is that the

effective difference in refractive indices will decrease causing the eigenmode profile will change.

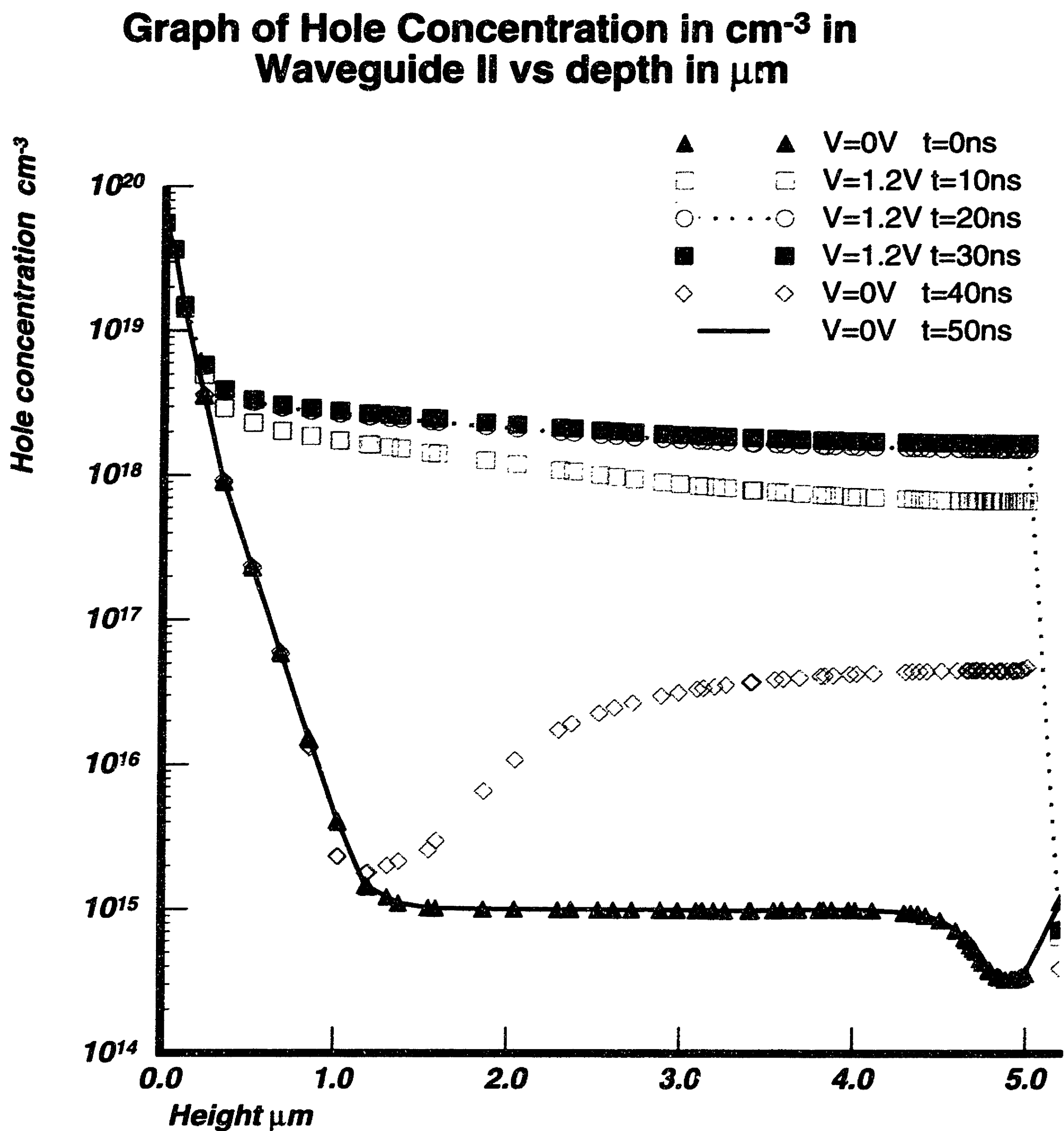

Figure 4.11: Simulation of hole concentration of the device in waveguide II. The applied voltage V=1.2V is turned at on $t=0^{+}$ns and then turned off at t=30ns. The system returns to V=0V state by t=50ns.

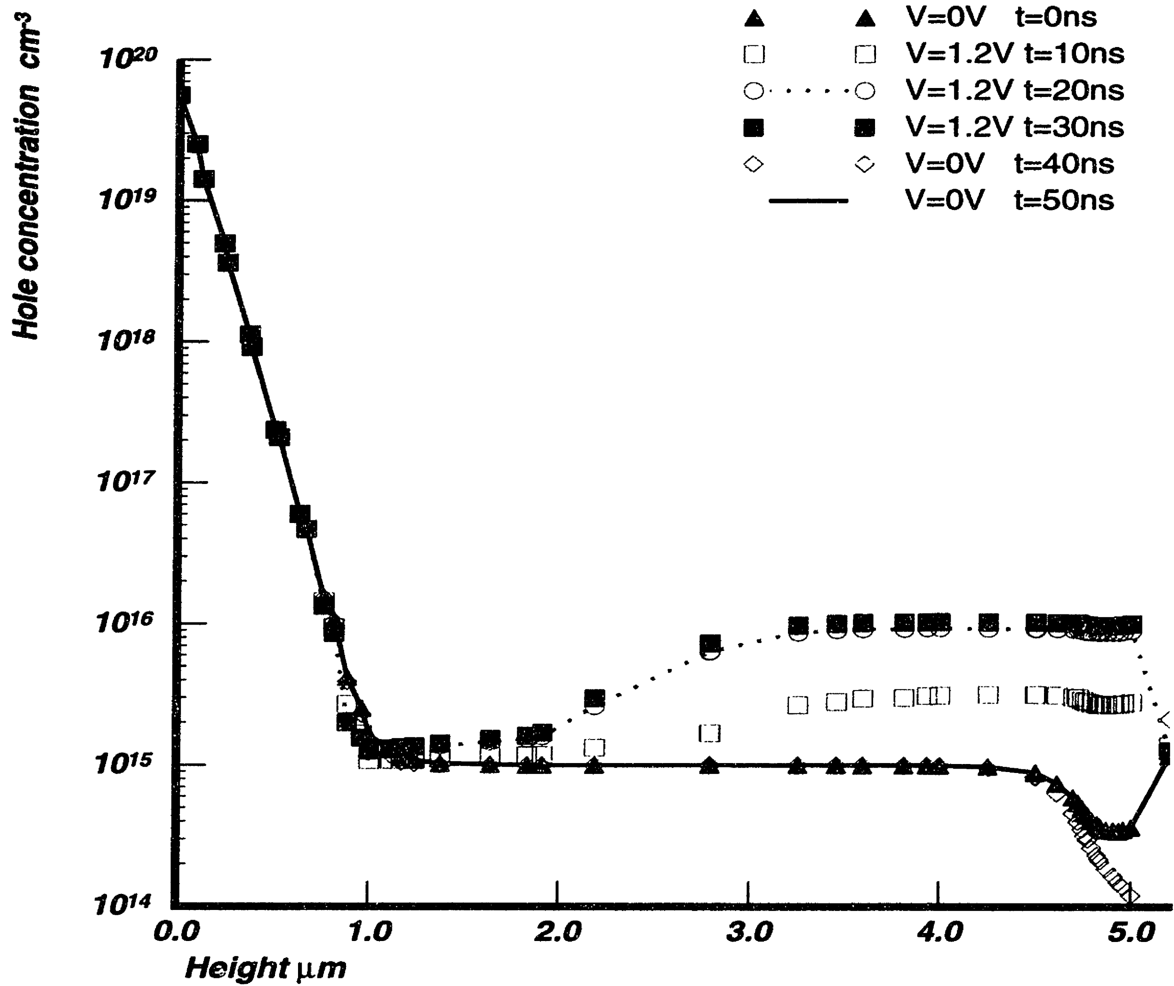

Figure 4.12: Simulation of hole concentration of the device in waveguide I. The applied voltage V=1.2 V is turned on at t=0^+ns and then turned off at t=30ns. The system returns to V=0V state by t=50ns.

One possible approach to solving the problem of carrier confinement, is to reduce the carrier lifetime in the silicon material bridging the gap between both ribs. Simulations indicate that the intrinsic minority lifetime of the carriers have to be reduced to 2×10^{-11}s, or 20 ps. A classic method of reducing the minority carrier lifetime is to use high dose MeV proton bombardment [43].Assuming a defect capture cross-section of $\sigma_d = 10^{-15}$cm^2

and a carrier thermal velocity on the order of $v_{th}=10^7$cm s^{-1}, the density of traps required to produce this lifetime is $N_t= 5x10^{18}cm^{-3}$, since the lifetime, is given [39] by

$$\tau_d = \frac{1}{\sigma_d N_t v_{th}} \qquad (4.2)$$

Thus, the MeV ion implantation will have to produce $5x10^{18}cm^{-3}$ defects in order to support this short carrier lifetime. This step limits the back end processing since these defects will anneal out high temperatures. A more efficient deep level defect which has a low diffusivity and higher annealing temperature should be found, to remove this limitation. Examples of such defects would Ti and Mo.

The modulator was simulated with the assumption that this sort of lifetime killing trap is possible. The switching speed of the modulator is on the order of 30 MHz, which would allow data rates of 30 Mbits/s. The total rise and fall time of the modulator is on the order 30 ns. The switching characteristics of the device are summarized in figure 4.11 and figure 4.12. As is apparent from the graph, the hole profiles stabilize approximately 15-20 ns after the voltage is switched on while the hole profiles require 10 ns to return to steady state conditions after the voltage is switched off.

The peak current required for this modulator is very large, approximately 0.706 A. The current density of the pin diode is approximately $4x10^4$ A cm^{-2} and the power dissipated by the device, is approximately 0.42 W. Although these figures are consistent with those cited by Sze [39], the current and power dissipation figures are large for a passive device. As the voltage is increased to 2 volts, the corresponding current increases to 3 A, the current density increases to approximately $2x10^5$ A cm^{-2} and the power dissipated by the device is 3 W. The way to decrease this large required current drive and power dissipation would be to reduce the size of the modulator. The large size of the modulator means that there is a large volume over which recombination occurs.

Another way to reduce to the power dissipation of the device, would be to reduce the separation within the guides. If the core separation of the guides could be reduced to 6.6 μm, the corresponding coupling length should be reduced to approximately 400 μm, which would correspond to a 30% decrease in total power dissipated just from the reduction in length alone. However, the narrower the separation, the harder it is to confine the waveguides. Thus a trade-off must be made.

Most of the processing but for the low dose MeV proton bombardment is compatible with standard VLSI processing techniques. If at the end of the process, there is no metal covering the trench between the two waveguides, it may be possible to use MeV proton implantation as the last step. In this case, the MeV proton bombardment will not affect any of the other steps.

4.2 Strip waveguide modulator

The strip waveguide coupling modulator was simulated with the dimensions of 0.2 μm x 0.5 μm and separations on the order of 0.1 μm as shown in figure 4.13. Similar curves can be obtained for any single mode rib waveguide system with a reasonable waveguide separation. As was the case with the rib waveguide, the simulations were run with the assumption that the initial beam was incident on the right waveguide and that the incident E field profile is the eigenmode of a single waveguide. The index change simulated was 3×10^{-3} to make the simulation consistent with the rib waveguide simulations.

As is expected, the coupling length is related exponentially to waveguide separation. The dimensions of the waveguide were 0.2 μm x 0.5 μm, optimal for propagation amongst the three strip waveguides that I have simulated earlier.

There is a trade-off to be made for the strip waveguide modulator. With both small and large waveguide separations, the required modulator length is relatively large and the

lithography would be extremely difficult since a separation of the order of tenths of μm has to be maintained over distances of 10^3 - 10^4 μm. If this separation is not maintained accurately, the light will not couple in the designed coupling length.

The reason why coupling in a strip waveguide is inefficient compared with a rib waveguide modulator is that the index difference between the core and cladding is large, so a change in index $\Delta n = 3x10^{-3}$ is not very significant. Thus, the effect of this change in index on the coupled waveguide eigenmode profiles is negligible. In addition, the change in the propagation constant is so small that its effect on the coupling length is very weak. Thus, the modulator requires a large interaction distance for modulation.

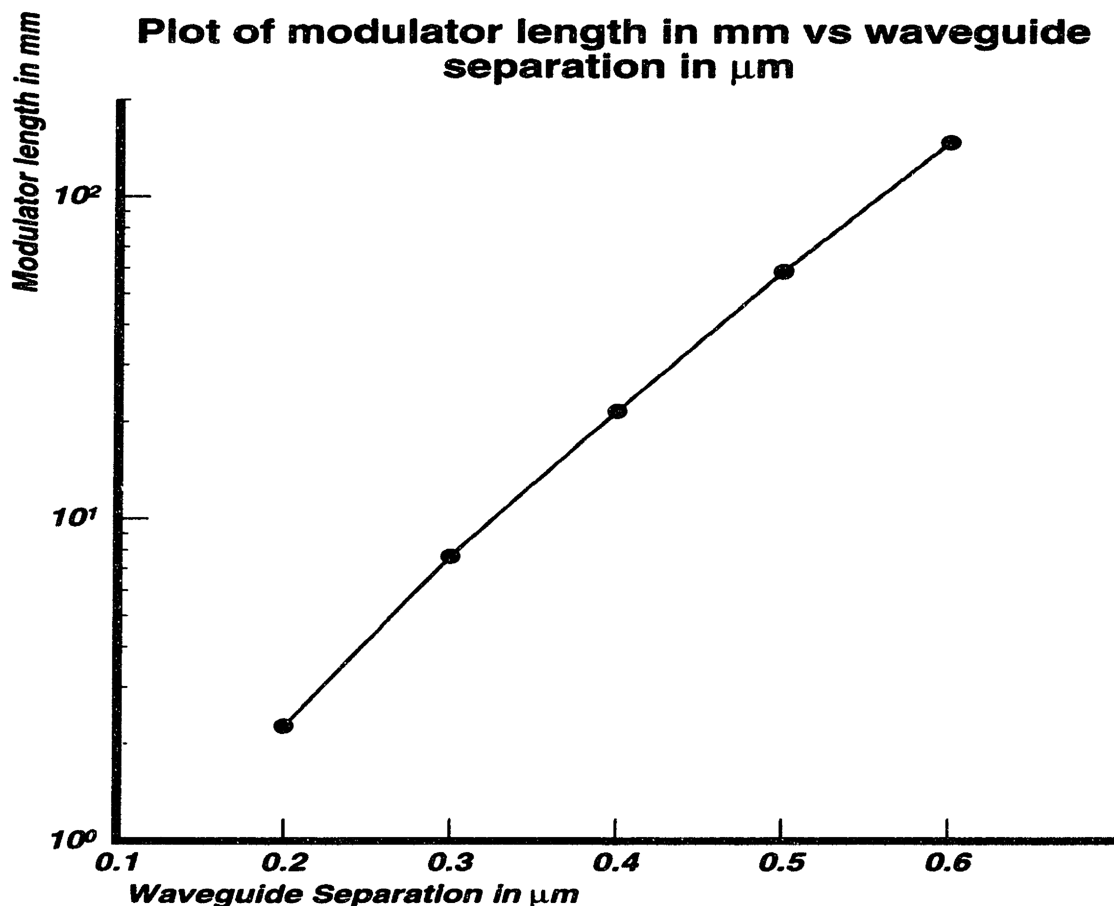

Figure 4.13: Plot of coupling length in μm vs. waveguide separation in μm for a strip waveguide coupler with strip dimensions 0.2 μm vs. 0.5 μm

As a result of this large coupling length for the strip waveguide, it would be more efficient and much easier to build an absorption modulator. An absorption modulator using the side contacts as mentioned in section 3.4.5 could be designed to achieve $10^{19}cm^{-3}$ electron and hole injection levels, providing an absorption coefficient of 150 cm^{-1}. For a 20 dB modulation depth, the necessary modulator length would be approximately 0.3 mm or 300 microns.

Chapter 5

Conclusion and Recommendations

5.1 Rib and Strip Waveguides

Rib and strip waveguides were evaluated as possible candidates for integration with a silicon electro-optic modulator. In order to evaluate their functionality in the modulator, the characteristics, loss and single mode constraints of these waveguides were explored using a beam propagation simulator. A rib structure of 5 μm x 3 μm with r=0.5 (rib height/ partially etched shelf height) was studied. Losses to the substrate and to metal contacts were shown to be small, but bending losses were found to be inconclusive.

Large dimension rib waveguides will be useful for chip to chip connection since the large cross sectional area of the eigenmode, will facilitate easy coupling of fields from the waveguide to the fibre and vice versa.

Single mode strip waveguides based on an SOI stack were shown to have very small dimensions -- for waveguide heights of 0.2 μm the width had to be 0.5 μm or less; for 0.3 μm the width should be 0.3 μm. In addition, the minimum thickness of the underlying oxide for the strip waveguide was found to be 7000Å in order to attain losses to the substrate on the order of 1 dB/cm. This oxide thickness is too thick for SIMOX technology, although other SOI technology maybe used. Furthermore, losses to any metal contacts from the waveguide were found to be high. However, these losses may be minimized by contacting to the side walls of the strip waveguide. On the other hand bending losses were shown to be low.

The small dimensions of the strip waveguides make them attractive for on chip optical interconnection. especially if LPCVD polysilicon on oxide technology is shown to be feasible. This technique will make fabrication of such interconnects trivial.

5.2 Modulators

Rib waveguide couplers were simulated using optical, process and electrical simulators. A device based on a rib waveguide with dimensions 5 μm x 3 μm and r=0.5 was simulated. Optical waveguide simulations have shown that it should be possible to fabricate modulators with lengths on the order of 1 mm. For a separation of 6.8 μm, the device length was 600 μm. The corresponding device length for a separation of 7 μm was 900 μm.

Process and electrical simulations of the device have shown that injection levels of over 10^{18} cm^{-3} are achievable in the core region in one waveguide, without a significant increase in the carrier density in the other waveguide. The simulated bias was 1.2 volts which is compatible with VLSI/ULSI technology. A theoretical switching frequency of 30 MHz is achievable with the device simulated. Unfortunately this is an extremely high powered device and it requires a large current to drive it.

Strip waveguide couplers were not simulated in great detail since the efficiency of the modulator is poor due to the strongly confined E field. An absorption modulator will probably be more efficient.

5.3 Future Work

The waveguides proposed here should be fabricated and their characteristics should be compared to the simulations. The rib waveguide coupler should also be fabricated to examine the feasibility of such a device. A strip waveguide absorption modulator should

It remains to be seen whether single mode waveguides can be optimized for silicon optoelectronics applications. There are several fundamental problems with single mode waveguides that must first be resolved before they can be used in real optoelectronics applications. First of all, end to end coupling losses due to the small core sizes must be

studied. The rib waveguide having a larger core, will have lower coupling losses than the strip waveguide. However the bending loss problem of the rib waveguide structure will have to be examined more closely in order for it to be useful. As for the strip waveguide, the high losses to metal contacts will be the major challenge. Another challenge would be the integration of all the necessary optoelectronics components, the source, waveguides and the detector. Silicon/silicon-germanium detectors for light at 1.55 μm have been proposed, and although light sources are being developed, they are far from being efficient devices. These have to be developed further before fully integrated optoelectronics applications on silicon can be considered.

5.3.1 Metal Contact vs. Bending Losses

Contacting to the rib waveguide is easy because the core area is large and the E field at the edge of the core is small. In addition, a second contact may be made to the cladding region because the cladding region is an oxide/silicon/air stack and a contact may be made to the silicon in the cladding. Unfortunately, this is not the case with the slab waveguide, and it is difficult to devise a contacting scheme on the silicon core that will result in low loss propagation.

On the other hand bending losses of rib waveguides are extremely large when compared to that of the strip waveguide because the bending in the rib waveguide occurs on the plane in which a large amount of the mode resides outside the core. The amount of power residing outside the core in the plane of bending, is very small for the strip waveguide resulting in low bending losses.

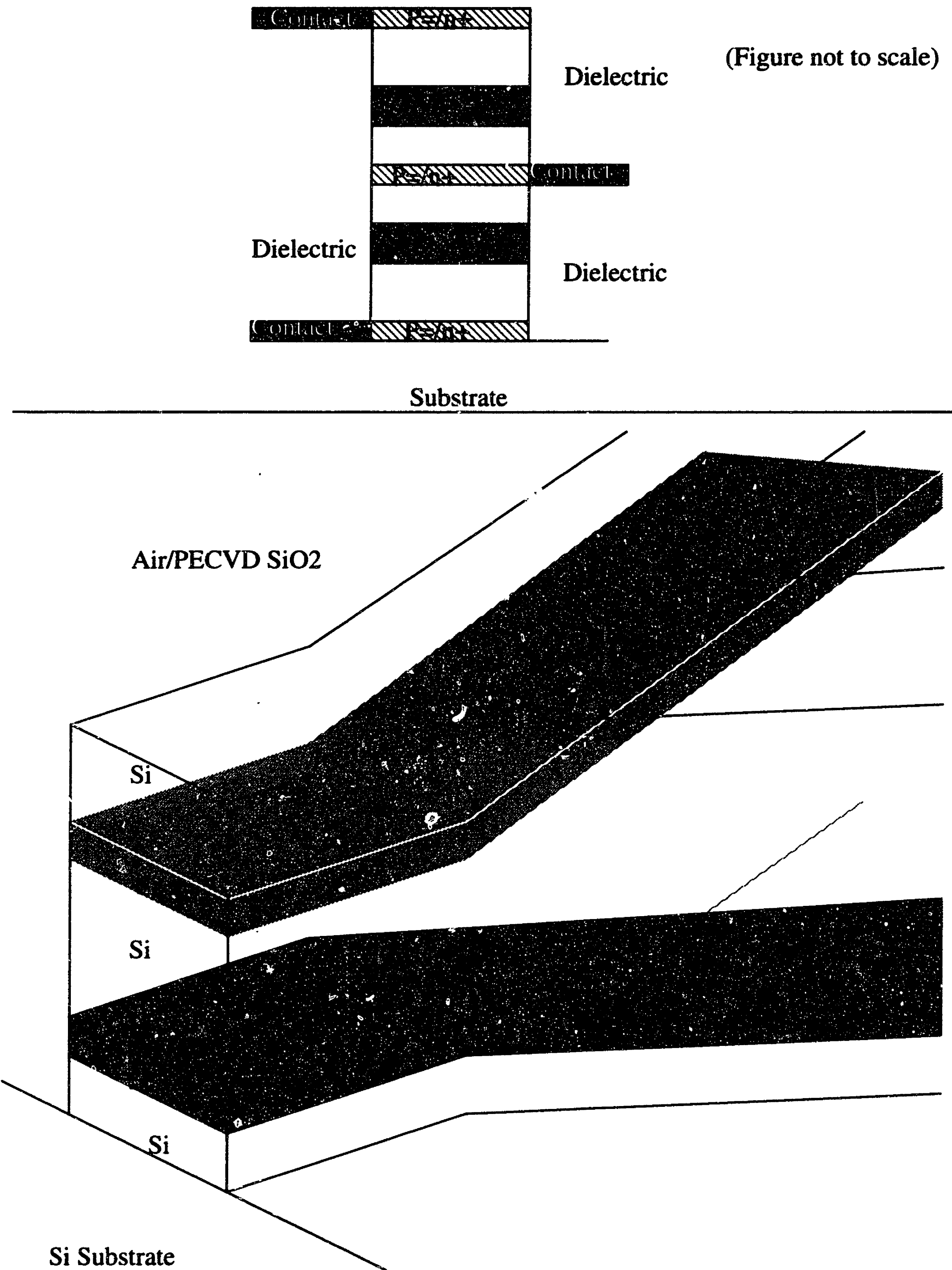

Figure 5.1: Schematic of SiGe in Si waveguides which should show low bending loss and loss to metal contacts

Since bends will probably have to occur parallel to the silicon substrate while contacting can be effected using vertical structures, I propose using single mode Si/SiGe/Si structures as shown in figure 5.1 as a possible waveguide system which would have low bending losses and low metal contacting losses. The width and thicknesses of the SiGe layer will be adjusted for single mode propagation [40]. If the buffer layers are made sufficiently lossy the higher order modes due to the finite silicon thickness can be made to decay away rapidly.

SiGe has a higher index of refraction than silicon and will therefore act as the core of the waveguide. If bending occurs parallel to the silicon substrate surface, the bending losses will be small and consequently small radii of curvature are possible, since the amount of the E field residing outside the core region and inside the dielectric cladding is small.

The metal contacts can be made on the silicon buffer layers which can be grown relatively thick to ensure that the field at the top and bottom surfaces are negligible. Contacts can then be made to these buffer layers with small optical losses, since the intensity of the fields overlapping contacts is small.

Finally the free carrier refraction effect can be used as a means to modulate the light.- The injection mechanism may be p-i-n diode injection similar to that described in the section 4.1.6 or some novel injection scheme for heterostructures, e.g. HBTs or FETs.

References

[1] R. Soref, "Silicon Based Optoelectronics", DOD Fiber Optics Conf. Proc., 1992.

[2] B. Zheng, J. Michel, F.Y.G. Ren, L.C. Kimerling, D.C. Jacobson and J.M. Poate, "Room temperature sharp line electroluminescence at $\lambda = 1.54$ µm from an Er doped, silicon light emitting diode", Applied Physics Letters, to be published.

[3] J. Michel, J.L. Benton, R.F. Ferrante, D.C. Jacobson, D.J. Eaglesham, E.A. Fitzgerald, Y.H.Xie, J. M. Poate and L. C. Kimerling, "Impurity enhancement of the 1.54-µm Er^{3+} luminescence in silicon", Journal of Applied Physics **70,** 2672, 1991.

[4] F.Y.G. Ren, J. Michel, Q. Sun-Paduano, B. Zheng, H. Kitigawa, D.C. Jacobson, J.M. Poate and L.C. Kimerling, "IC compatible processing of Si:Er for optoelectronics", MRS Proceedings, **301**, 87, 1993.

[5] J. Michel, F.Y.G. Ren, B. Zheng, D. C. Jacobson, J. M. Poate, and L.C. Kimerling, "The physics and application of Si:Er for light emitting diodes", Proceedings of ICDS 17.

[6] R. A. Soref and B. R. Bennett, "Electro-optical Effects in Silicon", IEEE Journal of Quantum Electronics, **QE-23**, 123, 1987.

[7] Institution of Electrical Engineers, Properties of Silicon, 1988.

[8] J.C. Bean, H. J. Leamy, J. M. Poate, G. A. Rozgonyi, J. P. van der Ziel, J. S. Williams and G. K. Celler, "Substrate doping effects upon laser-induced expitaxy of amorphous silicon", J. Appl. Phys. **50**, 881,1991.

[9] R. E. Jones Jr. and S. P. Wesolowski, "Electrical, thermoelectric, and optical properties of strongly degenerate polycrystalline silicon films", J. Appl. Phys **56**, 1701, 1984.

[10] D. M. Koker, Ph.D. thesis proposal, 1994, unpublished.

[11] C. K. Tang, G. T. Reed A. J. Walton and A.G. Rickman, "Simulation of a Low Loss Optical Modulator for Fabrication in SIMOX material", M.R.S. Symp. Proc, **298**, 247, 1993.

[12] R. A. Soref, J. Schmidtchen, and K. Petermann, "Large Single-Mode -Rib Waveguides in GeSi-Si and Si-on-SiO_2", IEEE J. of Quantum Electronics, **QE-27**, 1971, 1991.

[13] R. A. Soref and K. J. Ritter, "Silicon antiresonant reflecting optical waveguides", Optics Letters, **15**, 792, 1990.

[14] S. Giguere, L. Freidman, R. A. Soref and J. P. Lorenzo, "Simulation Studies of Silicon Electro-Optic Waveguide Devices", J. Appl. Phys. **68**, 4964, 1990.

[15] G. Cocorullo, F. Della Corte, I. Rendina and A. Cutolo, "New possibilities for efficient silicon integrated electro-optical modulators", Optics Communications, **86**, 228, 1991.

[16] T. Pirnat, L. Friedman and R. A. Soref, "Electro-optic mode-displacement silicon light modulator", J. Appl. Phys., **70**, 3355, 1991.

[17] H. C. Huang, S. Yee, R. B. Darling and C. H. Chan, "A silicon diverging beam modulator fabricated by part of metal-oxide-silicon process modules", J. Appl. Phys., **72**, 1992.

[18] R. Normandin, D. C. Houghton, M. Simard-Normandin and Y. Zhang, "All-optical silicon-based integrated fiber-optic modulator, logic gate and self-limiter", Can. J. Phys., **66**, 833, 1988.

[19] W. P. Huang, C. Xu, S. T. Chu and S. Chaudhuri, "The Finite-Difference Vector Beam Propagation Method: Analysis and Assessment" Journal of lightwave Technology, **10**, 295, 1992.

[20] S. Jungling and J. C. Chen, "A Study and Optimization of Eigenmode Calculations Using Imaginary-Distance Beam Propagation Method", IEEE Journal Quantum Electronics, To be published.

[21] D. Marcuse, "Bending Losses of the Asymmetric Slab Waveguide", Bell System Tech. J., **50**, 2551, 1971.

[22] E. A. J. Marcatili, "Bends in Optical Dielectric Guides", Bell System Tech. J., **48**, 2103, 1969.

[23] M. Heiblum and J. Harris, "Analysis of Curved Optical Waveguides by Conformal Transformation", IEEE J. of Quantum Electronics, **QE-11**, 75, 1975.

[24] G. H. Ames and D. G. Hall, "Attenuation in Planar Optical Waveguides: Comparison of Theory and Experiment", IEEE J. of Quantum Electronics, **QE-19**, 845, 1983.

[25] R. Baets and P. E. Lagasse, "Loss calculation and design of arbitrarily curved integrated-optic waveguides", Optical Society of America.

[26] R. J. Deri, R. J. Hawkins and E. Kapon, "Rib profile effects on scattering in semiconductor optical waveguides", Appl. Phys. Lett., **53**, 1483, 1988.

[27] M. Seto, R. J. Deri, A. Yi-Yan, E. Colas, W. J. Tomlinson, R. Bhat and A. Shahar, "Fabrication of Submillimeter Radius Optical Waveguide Bends with Anisotropic and Isotropic Wet Chemical Etchants", J. Lightwave Tech., **8**, 264, 1990.

[28] M. W. Austin, "GaAs/GaAlAs Curved Rib Waveguide", IEEE J. Quantum Electronics, **QE-18**, 795, 1982.

[29] E. F. Kuester and D. C. Chang, "Surface-Wave Radiation Loss from Curved Dielectric Slabs and Fibers", J. Quantum Electronics, **QE-11**, 903, 1975.

[30] A. Neyer, "Electro-optic X-switch using single mode Ti:$LiNbO_3$ channel waveguides", Electronics Lett., **19**, 553, 1983.

[31] O. Mikami and H. Nakagome, "Waveguided Optical Switch in InGaAs/InP using free carrier Dispersion", **10**, 229, 1984.

[32] C.R.C. Hand Book of Chemistry and Physics, ed. D. R. Lide, CRC Press, 1990-1991.

[33] Donald L. Lee, Electromagnetic Principles of Integrated Optics, John Wiley & Sons.

[34] H. A. Haus and C. G Fonstad, IEEE J. of Quantum Electronics, "Three-Waveguide Couplers for Improved Sampling and Filtering", **QE-17**, 2321,1981.

[35] H. A. Haus, Optics and Optoelectronics, 1986.

[36] H. A. Haus and W. P. Huang, "Coupled Mode Theory", Proceedings of the IEEE, **79**, 1505, 1991.

[37] A. Yariv, "Coupled Mode Theory for Guided-Wave Optics", IEEE Journal of Quantum ELectronics, **QE-9**, 919, 1973.

[38] E. A. J. Marcatili, "Dielectric Rectangular Waveguide and Directional Coupler for Integrated Optics", The Bell Systems Technical Journal, September 1969.

[39] S. M. Sze, Physics of Semiconductor Devices, Wiley Interscience 1971.

[40] F. Namavar and R.A. Soref, "Optical Waveguiding in $Si/Si_{1-x}Ge_x/Si$ Heterostructures", J. Appl. Physics, **70**, 3370,1991.

[41] C. S. Rafferty, PROPHET.

[42] M. R. Pinto, PADRE.

[43] D. Bielle-Daspet, L. Castaner, G. Gasset and M. Benzohra, "Changes in Lifetime and Diffusion Length due to the Electron and Proton Bombardment of Silicon Solar Cell", Solar Cells, **2**, 31,1980.